THE APPLICATION OF A CHARACTERIZED PRE-CLINICAL GLIOBLASTOMA ONCOSPHERE MODEL TO *IN VITRO* AND *IN VIVO* THERAPEUTIC TESTING

by
Kelli M. Wilson

A dissertation submitted to Johns Hopkins University in conformity with the requirements for the degree of Doctor of Philosophy

Baltimore, Maryland
March, 2014

ABSTRACT

Glioblastoma multiforme (GBM) is a lethal brain cancer with a median survival time (MST) of approximately 15 months following treatment. A serious challenge facing the development of new drugs for the treatment of GBM is that preclinical models fail to replicate the human GBM phenotype. Here we report the Johns Hopkins Oncosphere Panel (JHOP), a panel of GBM oncosphere cell lines. These cell lines were validated by their ability to form tumors intracranially with histological features of human GBM and GBM variant tumors.

We then completed whole exome sequencing on JHOP and found that they contain genetic alterations in GBM driver genes such as *PTEN*, *TP53* and *CDKN2A*. Two JHOP cell lines were utilized in a high throughput drug screen of 466 compounds that were selected to represent late stage clinical development and a wide range of mechanisms. Drugs that were inhibitory in both cell lines were EGFR inhibitors, NF-kB inhibitors and apoptosis activators. We also examined drugs that were inhibitory in a single cell line. Effective drugs in the PTEN null and NF1 wild type cell line showed a limited number of drug targets with EGFR inhibitors being the largest group of cytotoxic compounds. However, in the *PTEN* mutant, NF1 null cell line, VEGFR/PDGFR inhibitors and dual PIK3/mTOR inhibitors were the most common effective compounds.

Using active compounds from the single agent screen, we subjected two oncosphere cell lines to a drug combination matrix high throughput screen. Synergistic combinations were tested *in vivo* and a PIK3 inhibitor paired with three different drugs extended survival in the JHH-520 GBM model. This data shows that the JHOP is

amenable to a high throughput drug screening format and that future preclinical studies on active compounds found in these results may deliver promising therapeutic leads.

Advisor: Dr. Gregory J. Riggins

Readers: Dr. Gregory J. Riggins

Dr. Charles Eberhart

ACKNOWLEDGEMENTS

I first would like to thank my advisors, Dr. Gregory J. Riggins and Dr. Gary Gallia. Dr. Riggins was extremely supportive and always made himself available for me to discuss new data or ask advice about science and life. Dr. Gallia was an excellent source of knowledge about clinical issues related to my project and the precision he uses for critical surgeries extends to all areas of his life. I would also like to thank my committee members, Dr. Robert Casero and Dr. Charles Eberhart for their expertise and advice throughout my thesis project. I would also like to thank the Cellular and Molecular program Director, Dr. Rajini Rao, and the administrators, Colleen Graham and Leslie Litcher for keeping the best interests of CMM students at heart and for always providing me with anything I asked or did not ask for.

The members of the Riggins/Gallia laboratory were critical to the successful completion of my thesis and I cannot thank them enough for answering all my questions and providing me with a sense of family in lab. Dr. I-Mei Siu, Sasha Borodovsky, Tara Williamson, Dr. Zev Binder, Dr. Vafi Salmasi, Dr. Reny Bai, Dr. Avadhut Joshi, Dr. Kanlaynee Sawanyawisuth, Dr. Gilson Baia, Dr. Qi Zhao, Dr. Octavia Caballero, Dr. Verena Staedtke, Dr. Meghan Seltzer, Dr. Genevieve Weber, and Dr. Collette ApRhys. I owe an especially large debt to my close friends Sasha Borodovsky and Tara Williamson for all their help with animal experiments and daily lunch and snack breaks. Dr. Zev Binder was also of great importance to my thesis project, as he was responsible for the generation and validation of many of the oncosphere cell lines. I also am thankful for Dr. Qi Zhao, who completed the sequencing analysis for all the cell lines.

This project would not have been possible without great assistance from outside collaborators. Dr. Robert Strausberg of the Ludwig Institute for Cancer Research and Dr. Ewen Kirkness from the J. Craig Venter Institute made it possible for me to have whole exome sequencing done on my cell lines. I would also like to thank Dr. Lesley Mathews Griner, Dr. Craig Thomas, Dr. Marc Ferrer and other members of the National Institutes of Health/National Center for Advancing Translational Sciences (NIH/NCATS). They completed the qHTS drug screening which allowed this project to be more novel and impactful.

Lastly, I must thank my family and friends because they have provided me with the love and support necessary to achieve my dream. My CMM classmates have helped me remain sane during graduate school and I wish them all the best in their future endeavors. My mother and father have always been supportive of my goals even though they have not been down this road themselves. I owe an especially large thank you to my sister who has done more for me than she will ever know. Finally, my biggest supporter, my husband Kevin Wilson, has always believed in me even when I did not believe in myself. He has supported me even when he was at his lowest and I admire his strength and perseverance. Without his strength, I would not have achieved my dream. Thank you.

TABLE OF CONTENTS

LIST OF TABLES AND FIGURES

Chapter 1: Background and Review of Relevant Literature

Chapter 3: Results

1 Background and Review of Relevant Literature

History of GBM Therapeutics and Current GBM Clinical Trials

Malignant astrocytomas are the most common glial tumor type. Grade IV astrocytoma, more commonly known as Glioblastoma (GBM), is the most malignant glioma, and makes up 80% of the annual incidence of adult glioma in the United States. GBM is classified by the World Health Organization (WHO) as a diffusely infiltrative tumor with features including microvascular proliferation, nuclear atypia, mitosis, and regions of necrosis (Louis et al.). GBM can be further classified as primary or secondary according to common genetic mutations, which seem to separate into two distinct groups.

Primary GBM is defined as a tumor that arises de novo with no patient history of tumor and makes up 90% of CNS tumors in adults. GBM variants exist which are

classified by histological characteristics. Gliosarcoma is a rare variant that shows histological features of both glioma and sarcoma (Evanthia Galanis et al.). GBM can also contain areas of different tumor types. Primitive neuroectodermal tumor (PNET) can exist in a GBM, characterized by areas of multipotent embryonic cells (Perry et al.). Areas of oligodendroglioma, a glioma subtype composed of cells of oligodendroglial origins, can also be found in some GBMs(Louis et al.). Although histological differences define GBM variants, there is little or no difference in patient treatment between a pure GBM and a GBM variant. Tumor recurrence causes the death of the almost all GBM patients.

Due to limited treatment options, the median survival time for GBM patients is 14 -18 months following diagnosis (DeAngelis). The current standard of care for patients diagnosed with GBM is surgical resection followed by concomitant radiation therapy and oral temozolomide (Temodar® or TMZ) (Walker et al.) (Stupp et al.) Bis-chloroethylnitrosourea (BCNU) impregnated wafers, Gliadel, have also been shown to extend survival in patients with recurrent and newly diagnosed disease (Stupp et al.) (Gallia, S. Brem, and H. Brem). Although the Vascular Endothelial Growth Factor (VEGF) inhibitor Bevacizumab (Avastin®) provides clinical improvement, there is no clear evidence of a survival benefit with the addition of Bevacizumab (Lai et al.). Once GBM patients no longer benefit from the existing therapies, treatment options are normally limited to experimental therapies. Although many clinical trials have been attempted to generate new therapeutic options for GBM patients, few have demonstrated a statistically significant survival benefit.

The timeline of approved therapies for GBM has had large gaps of time without new developments. The first non-surgical treatment for GBM patients, radiation therapy, was approved in 1980. 25 years later, TMZ was approved followed by Avastin five years later. Numerous clinical trials have been performed, however very few have led to approved therapies with a significant survival benefit. Small molecule inhibitors have been tested in GBM but without great success. There are currently hundreds of small molecules in clinical trials for GBM, many of them within the same drug class (Table 1). The most common drug classes are traditional chemotherapeutic agents that have been successful in other cancers. All these clinical trials were initiated based on data from pre-clinical studies using GBM cell lines and animal models.

Table 1 – Small molecules that have been evaluated in clinical trials for GBM as listed on www.clinicaltrials.gov

Mechanism of Action/Drug Target	**Investigational Agents**
Topoisomerase Inhibitors	Irinotecan, Gimatecan, Topotecan, Etoposide, Camptothecin, Pyrazoloacridine, Karenitecin, Erinotecan, Astrasetecan, Acridine carboxyamide, Lucanthone, Edotecarin
Platinum containing compounds	Carboplatin, Cisplatin, Oxaliplatin
Anti-angiogenesis	Thalidomine, Lenalidomide
mTOR inhibitor	Sirolimus, Temsirolimus, Everolimus, AP25373, AZD8055, CC-223
EGFR Inhibitors	Erlotinib, Lapatinib, Gefitinib, Afatinib, AC4280, Dacomitinib, AEE788, ABT-414
VEGFR/PDGFR Inhibitors	Sunitinib, Sorafenib, Cediranib, Vandetanib, Pazopanib, Nintedanib, Vatalanib, Tandutinib, Cabozantinib, Axitinib, Crizotinib, PLX3397, Dovitinib, Crenolanib, SU5416, NVP-BGJ398, INC280, Tivozanib, E7050, E7080
HDAC Inhibitors	Vorinostat, Panobinostat, Romidespin, Entinostat
Farnesyl Transferase Inhibitors	Lonafarib, Tipifarnib, SCH66336
Bcr-Abl Inhibitors	Dasatinib, Imatinib, Bosutinib, Bafetinib
Anti-angiogenesis	Cilengitide, ABT-510
Alkylating agents	Cyclophosphamide, Busulfan, Melphalan hydrochloride, SarCNU, Fotemustine, VAL-083, Cloretazine, TH-302, Irofulven, Glufosfamide, Semustine
Ribonucelotide reductase Inhibitor	Motexafin gadolinium, gemcitabine
PKC inhibitor	Enzastaurin
Proteasome Inhibitor	Bortezomib
SMO receptor antagonist	Vismodegib, LEQ506
Microtubule stabilizer	Paclitaxel, TPI-287, Cabazitaxel, Docetaxel, MPC-6827, Epithilone, Ixabepilone, CYT997, Ortataxel
Anthracycline	Doxorubicin, RTA 744
Protease Inhibitor	Ritonavir, Lapinovir, Nelfinavir
Gamma secretase Inhibitor	RO4929097
Selective Estrogen Receptor Modulator	Tamoxifen, CC-8490
Retinoic Acid Receptor	Isotretonin
PIK3 Inhibitor	BKM120, Perifosine, XL147, PX866
O6-alkylguanine-DNA alkyltransferase	O6-benzylguanine
Calcium channel blocker	Carboxyamidotriazole Orotate

Pyruvate dehydrogenase Inhibitor	Dichloroacetic acid
TGF-β Kinase Inhibitor	LY2157299
Anti-metabolite	Capecitabine, 6-thioguanine, 5-fluorouracil, Cladribine, Alanosine, Mercaptopurine, Ara-C
Folate anti-metabolite	Pemetrexed, Methotrexate
Anti-malarial	Hydroxychloroquine
PIK3/mTOR Inhibitor	XL765, GDC-0084
Oxygen diffusing enhancing compound	Trans sodium crocetinate
Antiviral	Valcyclovir, Valgancyclovir
Retinoid derivative	Fenretinide
Ang1/Ang2 Inhibitor	Trebananib
Bcl2 Inhibitor	Gossypol
Alcohol dehydrogenase inhibitor	Disulfiram
AKT Inhibitor	MK-2206
NSAID	Celecoxib, Vioxx
Tetracycline antibiotic	Minocycline, Incyclinide
PBN derivative	OKN-007
Synthetic lipid	Minerval
Tropomyosin receptor kinase inhibitor	AZD7451
Tubulin polymerization Inhibitor	Mebendazole, Vinorelbine
Antimicrobial	Taurolidine
Benzodiazipine	ECO-4601
PARP Inhibitor	E7016, MK-4827, ABT-888, Olaparib
Cdk inhibitor	PD 0332991
MMP Inhibitor	Prinomastat
Stat3 Inhibitor	WP1066
DNA-PK/mTOR Inhibitor	CC-115
Wee kinase Inhibitor	MK-1775
PDE5 Inhibitor	Sildenafil
Angiotensin II Receptor Antagonist	Losartan

GBM Pre-clinical Models

In vitro and *in vivo* models of GBM are critical to the advancement of new drugs to human clinical testing. Glioblastoma cell lines are all generated from surgical specimens, however they differ in their culture conditions. GBM cell lines can be classified into two groups: adherent and oncosphere cell lines. Adherent cell lines are grown in media containing serum and cells grow as a monolayer that is adherent to the cell culture flask. Oncosphere cell lines are grown in media containing no serum and growth factors such as EGF and FGF. Oncosphere cell lines grow in suspension and form spherical groups of cells. Both cell types have advantages and disadvantages.

The commonly used adherent GBM cell lines are U87-MG, LN229, and T98G, all of which are available for purchase from American Type Culture Collection (ATCC) allowing for widespread use of these lines for research purposes. As of March 2014, ATCC has no GBM oncosphere cell lines available for purchase, which limits the widespread use of these cell lines. Oncosphere cells are seen as superior to adherent cell lines because within a spheroid, cells are in a three dimensional space and are exposed to differing amounts of oxygen, nutrients and drugs, much like an *in vivo* tumor (Santini and Rainaldi). Methods for generation and culture of GBM oncosphere cell lines were first published in 2002 and were shown to have the ability to express glial and neuronal markers (Ignatova et al.). While the creation of GBM oncosphere cell lines was published less than 15 years ago, these cell lines are only recently gaining widespread use. There are currently no GBM oncosphere cell lines available for purchase from the ATCC. Both these adherent and oncosphere cell lines can give rise to GBM in animals, however there are vast differences between the resulting tumors.

In vivo model systems for GBM therapeutic testing are a deciding factor in whether a drug is moved forward to clinical trials. Rodents with compromised immune systems are implanted with human GBM cell lines and tumors are allowed to grow. GBM tumors can be established in two locations on the rodent, subcutaneous or intracranial. Subcutaneous, or flank GBMs grow as a compact mass with no infiltration of surrounding tissue which is histologically unlike human GBM growth. Another disadvantage of using subcutaneous GBM models for testing of new therapeutics is they do not have a blood brain barrier (BBB). The ability of a compound to pass the BBB is a major consideration in human drug testing. Taken together, subcutaneous GBM models are a poor system for use in pre-clinical testing of new therapeutics.

Intracranial implantation of GBM cells is a superior model for pre-clinical testing for many reasons. First, the realistic drug delivery in intracranial models allow for determining if the systemically delivered drug is reaching its target at effective concentrations. Secondly, recent studies have shown differences between which type of GBM cell line used in intracranial models can dictate how closely the tumor replicates features of human GBM. Intracranial GBM tumors grown using oncosphere cell lines show histological features of human GBM such as neovasculature, mitotic figures and infiltrative tumor growth (Galli et al.). When U87-MG cells are grown intracranially, they grow as an intact mass that does not infiltrate surrounding brain tissue. Recent studies have shown that oncosphere cell lines generated from GBM variants, such as gliosarcomas, can replicate the histological features of these variants *in vivo* (Wakimoto et al.).

Another major advantage of oncosphere cell lines is that these cell lines maintain the genomic profile of the original tumor better than serum-grown adherent cell lines. Adherent and oncosphere GBM cell lines generated from the same tumor were genetically compared to the original patient tumor. Oncosphere cell lines maintained the original mutations, chromosomal aberrations, and transcriptional patterns present in the original tumors (J. Lee et al.). Adherent cell lines were found to have de novo point mutations, significant increases in chromosomal numbers and vastly different transcriptional patterns compared to the original tumors. Taken together, research has shown that GBM oncosphere cell lines are a superior *in vitro* and *in vivo* model due to their ability to maintain the genotype and phenotype of the original patient tumor.

PIK3 and Ras Signaling Pathways

The PI3K pathway is controlled in part by Receptor Tyrosine Kinases (RTKs) located on the cell surface which transmit intracellular growth signals. Upon binding of a particular ligand to the RTK, an autophosphorylation event occurs on the intracellular domain of the RTK resulting in exposure of phosphotyrosine residues. This allows for the binding of phosphatidylinositol 3-Kinase (PI3K) to the intracellular portion of the RTK through its Src Homology 2 (SH2) domain. Activated PI3K can then phosphorylate phosphatidylinositol (4,5)-bisphosphate (PIP2) into phosphatidylinositol (3, 4, 5)-trisphosphate (PIP3). The presence of PIP3 on the plasma membrane allows inactive AKT to translocate to the plasma membrane where it binds PIP3 through its plexstrin homology (PH) domain. This translocation is sufficient to allow for phosphorylation of AKT (Andjelkovic et al.). Pyruvate dehydrogenase kinase 1 (PDK1) and other kinases can now phosphorylate AKT at the T308 and S473 sites, which fully activate AKT.

PhosphoAKT can now phosphorylate many other downstream targets, which are involved in the regulation of cell growth and survival. The main negative regulator of AKT signaling is Phosphatase and Tensin Homologue (PTEN). PTEN is an enzyme that is able to turn off AKT signaling by dephosphorylating PIP3 to create PIP2 which blocks the binding of AKT thereby turning off activation of AKT which blocks phosphorylation of downstream targets. Downstream targets of AKT include GSK-3β, MDM2, mTOR, BAD and FoxO proteins (Datta et al.) (Diehl et al.) (Mayo and Donner) (Cai et al.) (Biggs, Cavenee, and Arden) (Brownawell et al.). The entire PIK3 pathway is shown in Figure 1. This pathway is crucial to cell growth and also plays a role in the ability of the cell to undergo apoptosis (Datta et al.; Dudek et al.).

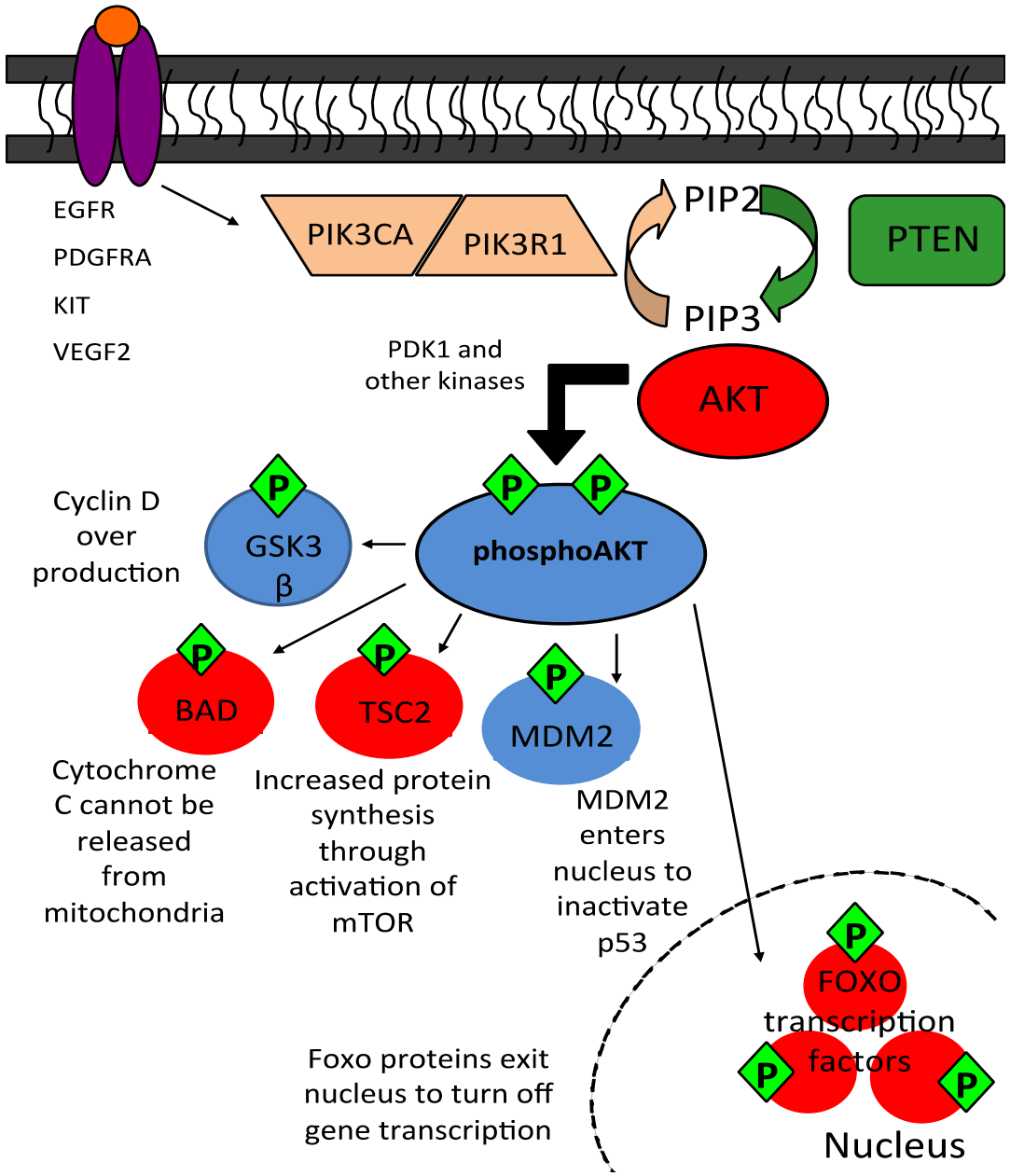

Figure 1 – The PIK3/PTEN signaling pathway.

This pathway is frequently mutated in GBM causing elevated phosphoAKT levels. The end result of this is a cell that has self-sufficiency in growth signals, is insensitive to anti-growth signals, has limitless replicative potential and can evade apoptosis. Red indicates inactive proteins and blue indicates active proteins.

The Ras/Raf/MAPK pathway is initiated by Receptor Tyrosine Kinases (RTKs) on the cell surface, in the same way as the PIK3 pathway. The binding of ligand to the extracellular portion of the receptor triggers an autophosphorylation event on the intracellular domain. This exposes phosphotyrosine residues that allow for binding of proteins such as Growth factor receptor-bound protein 2 (GRB2) through its SH2 domain. GRB2 is an adaptor protein with an Src homology 3 (SH3) domain, which allows for binding of other signaling proteins with an SH3 domain. Son of Sevenless (SOS) binds to GRB2 and this binding sets up the needed components to activate Ras. Ras is a G protein that is activated by binding GTP. SOS is a guanine nucleotide exchange factor (GEF) that binds to Ras-GDP and exchanges the GDP for GTP. Ras-GTP is active and can then go on to activate other downstream proteins. Ras-GTP is inactivated by the hydrolysis of GTP to GDP. Proteins with GTPase Activating Protein (GAP) function, such as Neurofibromin 1 (NF1), facilitate this process. Since NF1 is able to inactivate Ras-GTP, it serves as a critical negative regulator of the Ras pathway. This cycle of switching from active Ras-GTP to inactive Ras-GDP and back drives downstream signaling events. Ras-GTP can activate Raf kinases that will phosphorylate downstream kinases to activate a Mitogen Activated Protein Kinase (MAPK) cascade. The first protein in the MAPK cascade is MEK or MAPKK. After MEK is phosphorylated, it will then phosphorylate ERK. ERK will then phosphorylate more proteins such as RSK and transcription factors such as CREB. The entire Ras pathway is shown in Figure 2. The overall result of this signaling pathway on the cell is to activate cell growth pathways. Proteins in both the PIK3 and Ras pathways are frequently altered in GBM and this causes uncontrolled cell growth and an inability to undergo apoptosis.

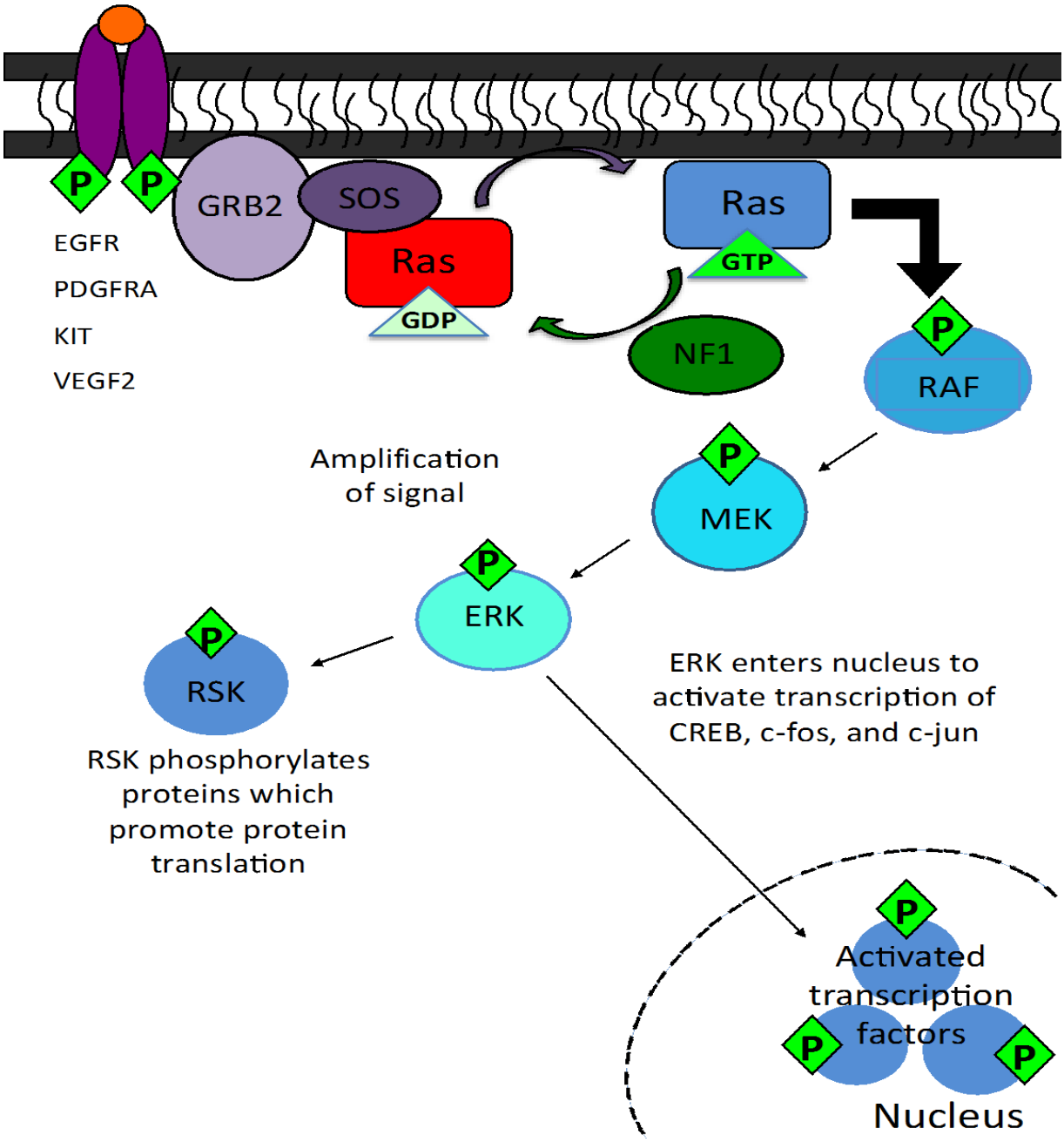

Figure 2 – The Ras/Raf/MAPK signaling pathway.

This pathway is frequently overactive in GBM due to loss of NF1 which causes the cell to have consistent activation of growth signals and limitless replicative potential. Red indicates inactive proteins and blue indicates active proteins.

Signaling Pathway Mutations in GBM

High throughput analyses of the glioblastoma genome have been used to discover the mutations that are most likely driving tumor cell growth. A comprehensive study of the glioblastoma genome was completed by extensive sequence analysis of over 20,000 protein coding genes in 22 GBM tumor samples (Parsons et al.). Genes with alterations in at least two of the 22 samples were then assessed in 83 additional GBMs. Additional copy number and gene expression analysis was integrated with the mutation data to form a list of GBM candidate cancer (CAN) genes. These 10 GBM CAN genes were the most frequently mutated and were more likely to be drivers of GBM cell growth. Another study completed copy number, gene expression and DNA methylation analysis on 206 glioblastoma samples. Of these, 91 samples also underwent mutational analysis (McLendon et al.). Both these studies found similar genes to be frequently altered in GBM. Many of these frequently altered genes were found to be players in the PIK3 Pathway and the Ras pathway.

Many different RTKs can activate the PI3K and Ras pathways. *EGFR* is amplified in about 36% of glioma samples (Rao et al.) with a further rearrangement of the amplification in about a third of cases yielding an internally deleted novel protein, such as EGFRvIII (a.k.a delta EGFR) (Wong et al.). The EGFRvIII mutation is a large deletion of the kinase domain of EGFR, which creates a constitutively active form of the receptor in the absence of EGF binding. Although EGFR is the most commonly mutated oncogene in GBM samples, other RTKs are amplified in GBM. A survey for mutations in the kinase domains of 20 RTK genes in glioblastoma samples found mutations in Platelet Derived Growth Factor Receptor Alpha (*PDGFRA*) and Fibroblast Growth

Factor Receptor 1 (*FGFR1*). Neither of the mutations was found to be activating, however the downstream effects of these mutations was not explored in this study (Rand et al.). Another study found *KIT*, Vascular Endothelial Growth Factor 2 (*VEGFR2*) and *PDGFRA* amplification in 47%, 39% and 29% of 43 primary glioblastoma samples, respectively (Joensuu et al.) /*FGFR1* was shown to have point mutations in GBM tumor samples and later was it was shown that disruption of Fibroblast Growth Factor (FGF) signaling suppresses GBM cell growth (Loilome et al.). Early studies showed that glioma cell lines express basic Fibroblast Growth Factor (bFGF) and grow in response to bFGF (Morrison, Yamaguchi, et al.). Further studies showed the FGFR1 mRNA and protein levels are highly expressed in GBM tumor samples (Morrison, Giordano, et al.). Taken together, these studies indicate that many different RTKs are amplified in GBM.

Once the RTK binds its ligand, the next step in the PIK3 pathway is activation of PI 3-kinase, which contains a catalytic and regulatory subunit, p110 and p85, which are products of the *PIK3CA* and *PIK3R1* genes, respectively. The p85 domain allows binding of PI 3-kinase to the phosphotyrosine residues on the intracellular domain of the RTK and the p110 domain catalyzes the phosphorylation of PIP2 into PIP3. Both of these genes were identified in the mutational analysis of the glioblastoma genome as drivers of GBM cell growth (Parsons et al.; McLendon et al.). Many large mutational analyses have been done to find PIK3CA mutations in glioblastomas (Samuels et al.; Broderick et al.; Mueller et al.; Hartmann et al.; Knobbe, Trampe-Kieslich, and G. Reifenberger; Gallia et al.) although few of these studies were able to identify activating mutations. Following PI 3-kinase activation, PIP3 becomes abundant on the plasma membrane and AKT can translocate and bind to PIP3. Surprisingly, activating mutations

in AKT itself are very rare in gliomas, however amplification of AKT have been found in some GBM samples (McLendon et al.).

A major regulator of AKT signaling is the PTEN gene. PTEN was first shown to be mutated in GBM and other cancers in 1997 (Li, Yen, et al.). It was identified as a tumor suppressor gene in gliomas in 1998 (Cheney et al.). In the same year, PTEN was shown to inhibit phosphoAKT and block programmed cell death by introducing wild type PTEN in glioma cell lines that previously lost PTEN expression (M. A. Davies et al.). A similar result was found when tumors formed after glioma cell lines were introduced into the flank of a nude mouse (Cheney et al.). Later studies showed that PTEN acts as a tumor suppressor by inducing apoptosis in normal cells that have DNA damage (Li, Simpson, et al.). However, the mechanism of how PTEN blocked AKT activation had yet to be elucidated. It was first shown that PTEN dephosphorylated PIP3 (Maehama and Dixon). In 1999, it was discovered that PTEN's regulation of PIP3 levels in the cell controls activated AKT ability to phosphorylate downstream targets (Sun et al.). Further studies showed that while PTEN is a tumor suppressor gene, loss of PTEN results in activated AKT, an essential outcome that creates an oncogenic signal within a cell (Stiles et al.). It was shown in glioma cell lines that expression of PTEN resulted in a decrease in phosphoAKT and re-expression of wild type PTEN increased the number of apoptotic cells. This indicates that when phosphoAKT levels are low, like in a cell with wild type PTEN expression, glioma cells are able to undergo apoptosis. However, if PTEN function is lost, then phosphoAKT levels can remain elevated and the cell will be unable to undergo apoptosis (M. A. Davies et al.). The overall effect of activating mutations in

various RTKs, PIK3CA, and loss of PTEN expression is elevated phosphoAKT levels which pave the way for a normal cell to acquire oncogenic traits.

The Ras pathway has been studied in glioblastoma, however less extensively than the PTEN/PIK3/AKT pathway. The initial genes involved in the Ras pathway are HRAS, KRAS and NRAS. Early studies of RAS mutations established that these mutations were not present in GBM cell lines and tumor samples (Bos). Another study of Ras expression in malignant astrocytoma found increased levels of Ras-GTP in glioma cell lines and tumor samples compared to normal astrocytes, however no activating mutations were found in any Ras genes (Guha et al.). A later study showed that induction of constitutively active Ras in glioma cell lines caused the cells to undergo cell death that was physically distinct from apoptosis (Chi and Kiatanka). The creation of genetically engineered mouse models of glioblastoma found that constitutive activation of KRAS and AKT are required for glioblastoma formation in mice (Holland et al.). This was the first study showing the importance of Ras activation in glioblastoma cell growth in an *in vivo* system. This was followed by a study that examined mutations in HRAS, KRAS, NRAS in 94 glioblastoma samples found two samples with mutations in NRAS (Knobbe, Trampe-Kieslich, and G. Reifenberger). Recent studies found that RAS genes were mutated in only 2% of 91 GBM tumor samples (McLendon et al.) but these alterations were not drivers of GBM growth. Overall, the presence of RAS gene mutations in glioblastoma is very low, however Ras activation is required for gliomagenesis *in vivo*. This has been explained by the prevalence of EGFR, PDGFR and MET amplification in GBM that would keep Ras in an activated state.

The RAF kinase gene family contains three members: ARAF, BRAF and RAF1. Of these genes, BRAF is most frequently mutated in human cancers (H. Davies et al.). BRAF mutations are found in GBM but at a low incidence. The first mutational study of BRAF in glioblastoma found three samples with BRAF mutations out of 94 examined (Knobbe, J. Reifenberger, and G. Reifenberger). The first assessment of copy number alterations in RAS/RAF genes in glioblastoma samples found that 76% contained gains in BRAF (Jeuken et al.) The high incidence of BRAF amplification is likely due to the location of the gene on chromosome 7, which is frequently amplified in GBM. Further studies showed that constitutive activation of RAF1 and AKT caused formation of glioblastomas *in vivo* (Lyustikman et al.; Robinson et al.). Taken together, these studies show that BRAF mutations in GBM are rare however amplifications can be found which would cause over activation of the Ras/Raf pathway.

A critical regulator of the Ras/Raf pathway is the NF1 gene. The link between NF1 and astrocytoma has been heavily explored due to the inherited disease Neurofibromatosis. Dr. Freiderich Daniel von Recklinghausen first described this disease in 1882. The autosomal dominant disease is characterized by small tumors that develop on nervous tissue and the development of tumors of the central nervous system. The NF1 and NF2 gene loss were found to be the cause of Neurofibromatosis Type 1 and Type 2, respectively. The NF1 gene was found early on to be frequently lost in astrocytomas (el-Azouzi et al.) and was hypothesized to be a tumor suppressor gene. A later study found NF1 to be mutated in a small number of glioblastomas (Thiel et al.). A genetically engineered mouse model of glioblastoma was developed using a mutant NF1 and mutant TP53 (Reilly et al.) (Zhu et al.). Genomic studies revealed that NF1 is frequently lost or

mutated in 15-18% of glioblastomas (Parsons et al.; McLendon et al.). The overall effect of amplified RTKs and loss of NF1 causes the Ras pathway to be overactive causing the GBM cell to have uncontrolled cell growth.

Hypothesis and Research Summary

Our hypothesis is that glioma oncosphere cell lines are a better pre-clinical model than traditional adherent cell lines. We believe that using these cell lines for testing new GBM therapeutics will lead to more successful clinical trials. To test this hypothesis, we generated nine oncosphere cell lines and completed whole exome sequencing on them. This analysis revealed the genomic profile in each cell line and allowed us to determine the best therapeutic targets. Two cell lines were selected for a high throughput drug screen of 466 drugs. We found that certain drugs were very efficacious in both cell lines however a large group of drugs were effective in only a single cell line. Top hits from this screen were selected for a matrix combination screen to determine what drugs have synergy in combination with each other. Two cell lines underwent this matrix screen and data showed that the most effective combinations involved a drug that inhibits members of the PIK3 or Ras pathway paired with a drug that inhibits a vital cellular process. These combinations were tested *in vivo* and a significant extension of survival was found in three different drug combinations. This research is the first full genomic characterization of a panel of glioma oncosphere cell lines and the first use of glioma oncosphere cell lines in a matrix combination drug screen.

2 Materials and Methods

Oncosphere Cell Line Generation

Patients with a suspected GBM were identified prior to their surgery at Johns Hopkins Hospital and patient demographics were obtained using the Electronic Patient Records (EPR) system through an IRB approved protocol. Tumor tissue was collected from the operating room during tumor resection and was transported to the laboratory on ice in a sterile container. Tissue was processed in sterile conditions. After a PBS rinse, a tissue chunk was frozen for storage in the tumor bank and the remaining tissue was used for cell line generation. First, the tissue was dissociated using the two scalpel method until it reached liquid consistency.

The sample was further dissociated using a glass tissue douncer followed by passage through a 16 gauge needle using added Minimal Essential Media (MEM). The

sample was then incubated at 37°C with collagenase (10mg/mL in HBSS) for 15 minutes. Next, the sample was passed through a pre-wetted 70 micron filter and the filter was washed with MEM to ensure all cells were filtered. This liquid was then centrifuged at 180 x g for 5 minutes to pellet the cells. If excess red blood cells were present in the cell pellet, red blood cell lysis buffer (BD #555899) was added to the pellet. The sample was incubated in the dark for 15 minutes at room temperature.

Cells were then pelleted and the supernatant was removed. The pellet was resuspended in 1mL of PBS with 1% fetal bovine serum (Gemini, Sacramento CA) in preparation for centrifugation using a sucrose gradient. 1mL of 30% sucrose was added to the sample and centrifuged at 3,100 x g at 4°C for 20 minutes. Supernatant was removed from the pellet and discarded. JHH-505 and JHH-520 did not undergo red blood cell lysis or sucrose centrifugation. The final cell pellet was resuspended in 10mL of complete Neurocult media (StemCell Technology #05751, Vancouver, BC) supplemented with EGF (20ng/mL in PBS, Peprotech #AF-100-15 Rocky Hill, NJ), FGF-b (10ng/mL in PBS Peprotech #100-18B) and 0.2% heparin (StemCell Technology #07980) and placed in a T75 cell culture flask.

Cells were grown in a humidified incubator at 37°C with 5% CO_2 and were monitored for oncosphere formation. Cell culture flasks were supplemented with 1mL of complete Neurocult media every 48-72 hours to prevent depletion of nutrients and growth factors. If oncospheres were observed, cells were passaged as described previously (Bakir et al.). Cell lines were considered stable after four to seven passages and were then subjected to additional validation experiments.

Cell Culture Methods

Br23C, JHU-0879, JHH-136, JHH-68, JHH-227, JHU-1016B, JHH-505 and JHH-520 were created in the Riggins lab. The cell lines with a JHH designation were collected using an unconsented patient protocol, so samples were de-identified upon collection. Cell lines with a JHU designation were collected using a consented patient protocol, which allowed for collection of two vials of blood from the patient and patient identifiers were associated with the sample collected. HSR-GBM1 cells were a gift from Sara Piccirillo and Angelo Vescovi to the Riggins lab. All cell lines were grown in suspension in Neurocult Stem Cell media containing EGF, bFGF and heparin using standard incubator conditions.

Oncosphere Cell Line Validation

Validation of each cell line began by doing Short Tandem Repeat profiling on each cell line. A Qiagen DNeasy kit (Qiagen, Valencia, CA) was used to extract genomic DNA and DNA concentration was determined using a Nanodrop 2000 (Thermo, Pittsburgh, PA). DNA was then aliquoted at 10ng/μL and sent to the Johns Hopkins Microarray Core Facility for STR profiling. The StemElite ID system (Promega, Madison WI) was used for STR profiling and controls included HeLa, K562 and mouse markers.

In vivo tumor formation was the second validation criteria for each cell line. 5-6 week old female athymic nude mice (NCI, Frederick MD) were used as previously described (Lee et al, 2006). Mice were anesthetized using a ketamine/xylazine mixture. 250,000 to 500,000 cells were dissociated into single cell suspension then injected into the striatum of two to four mice using a stereotactic frame. Surgical wounds were closed

using staples. Animal weight was monitored weekly and animals were euthanized upon signs of neurological defects such as rapid weight loss, hunching and difficulty with movement. Brains were removed and fixed in formalin for 24-48 hours then embedded in paraffin, sectioned and placed on slides. H&E staining was done on all samples and each slide was examined for histological features of GBM by board certified neuropathologists. For GBM variant tumors, the original primary tumor slides were compared to the xenograft for similarities.

Exome Capture and Next Generation Sequencing

DNA was extracted from nine oncosphere cell lines using a Qiagen DNeasy Miniprep Kit. For JHU-0879, JHH-136, JHH-68, JHH-227, JHU-1016B, JHH-505, and JHH-520, DNA was extracted from cells that were less than 15 passages from the passage number used for *in vivo* tumor establishment. Br23C and HSR-GBM1 are frequently used for *in vivo* experiments so any available cells were used without regard for passage number. JHU-0879 and JHU-1016B matched normal DNA was extracted from whole blood using a Qiagen DNeasy Blood and Tissue Kit. The STR profile of each sample was determined prior to sequencing to ensure each sample was independent. The amount of DNA in each sample was quantified using a Nanodrop Spectrophotometer. Library construction was completed at Johns Hopkins Microarray Core Facility. Genomic DNA fragmentation was performed with the Bioruptor (Diagenode), and size selection at 200 bp - 300 bp was carried out. The exomes of gDNA were captured using the Agilent SureSelect All Exon 50Mb Target Enrichment kit according to the manufacturer's instructions. The exomes of gDNA were captured using the Agilent SureSelect All Exon 50Mb Target Enrichment kit according to the manufacturer's instructions. The captured

DNA was sequenced on the Illumina HiSeq2000 platform according to the manufacturer's instructions, to generate 100-base paired-end reads. Image analysis and base calling were performed using Illumina's Casava1.8.2 software

Reads Mapping and Variant Identification

Reads were mapped to the human genome (GRCh37) using the Burrows-Wheeler Aligner (BWA) (PMID:19451168) version 0.5.9 with q=20. The resulting SAM (Sequence Alignment/Map) files were converted to BAM files, and sorted with SAMtools (PMID:19505943 v 0.1.18). PCR and optical duplicates, and multiple reads likely to be derived from a single cluster on the flow-cell image, were marked with Picard tools (v. 1.64). Regions that could benefit from realignment were identified using the GATK (PMID:21478889: v 1.0.5506) Realigner Target Creator. The reads covering localized indels were realigned, and quality values were recalibrated using GATK. The GATK (v. 1.5) was also used to locate, filter and annotate variants. Somatic changes including point mutations and small indels were called based on comparison between case and control. Only missense mutations were assessed for functional impact by PhyloP, SIFT, Polyphen, and Mutation Taster (Schwarz et al.) [8] programs.

Evaluation of Copy Number Alteration

Mean exonic coverage was calculated for all exonic baits in case and control samples by GATK. The mean exonic coverage of each exon was subsequently normalized by average whole-exome coverage of the sample. Individual case vs. control $\log_2$ ratios were then calculated for all the exons in the data set and plotted. The presence of copy-number alterations was detected using a combined approach involving a set of

statistical Wilcoxon signed-rank tests performed on a 500,000 bp sliding windows along the genome. Only genetic amplifications of greater than 10 copies are reported.

Immunoblotting

Oncospheres were dissociated into single cells then pelleted by centrifugation at 300xg for 5 minutes. Media was discarded and pellets were washed using PBS and centrifuged at 300xg for 5 minutes. Following removal of PBS, an appropriate volume of ice cold RIPA buffer containing protease and phosphatase inhibitors was added to the pellet. Following a 30 minute incubation on ice, cells were centrifuged at 14000 RPM at 4°C for 15 minutes. Supernatant was collected and protein levels were quantitated using a Pierce BCA assay kit (Thermo). 20ug of denatured protein was loaded on a 10% polyacrimide gel. The gel was run at 80V for 90 minutes using MES running buffer. Proteins were transferred to a PVDF membrane at 30V for 90 minutes at 4°C. Membrane was blocked in 5% milk-TBST mixture for 60 minutes at room temperature. Primary antibody incubation occurred overnight at 4°C and secondary antibody incubation was for 60 minutes. Membrane proteins were visualized using Pierce Chemiluminscence kit (Thermo) and film capture.

Quantitative High Throughput Single Agent Drug Screening

The Mechanism Interrogation PlatE is a collection of 466 small molecules that target signaling pathway components that are altered in many different cancers. Most of the MIPE compounds are in various stages of preclinical testing, clinical trials or FDA approved. The qHTS was completed using a 48 hour cell proliferation assay measuring cellular ATP content and was performed in a 1536 well microplate. High base solid

bottom white Grenier plates (#789173) were used throughout. JHH-136 and JHU-1016B were dissociated into single cells during their log growth phase then plated at 500 and 1000 cells per well in 5 μL of NeuroCult Media using a Multidrop liquid dispenser (Thermo). Next, a Pintool dispenser (Kalypsis) was used to add 23 nL of MIPE titrated compounds to columns 5 to 48. Columns 1 and 2 contained DMSO and columns 3 and 4 contained the proteasome inhibitor bortezomib at a final concentration of 9.2 μM which was used as a positive control for data normalization to induce complete cell killing. The remaining columns contained each drug in eleven different concentrations in order to obtain a dose response curve. Plates were then incubated for 48 hours with low evaporation stainless steel lids in standard incubator conditions. For cell viability measurements, 3 μL per well of CellTiter Glo reagent (Promega) was dispensed using a Bioraptor liquid dispenser (BD). After incubation for 15 minutes at room temperature, the luminescence signal was measured using a ViewLux CCD-based multi-label reader (Perkin Elmer). Cell growth values normalized to the DMSO only control values as a 100% activity, and bortezomib control as 0% activity. Curve Response Class analysis using algorithms developed at NGCG (Inglese et al.; Yasgar et al.) were used to fit the qHTS data to dose response curves and determine potency (IC_{50}) and efficacy (% max response) parameters for each compound tested. The drug screen was completed in duplicate for each cell line and dose response parameters obtained were averaged across each independent experiment.

Single agent Hit Verification and Secondary Screening

BIIB021, Obatoclax, and Bardoxolone methyl were selected for verification using a non-qHTS format. JHH-136, JHU-0879, HSR-GBM1, Br23C, JHH-227 and JHH-520

were dissociated during the log growth phase and was plated at 1000 cells per well in 178 μL of Neurocult media into a clear bottom 96 well plate. Following an overnight incubation at standard incubator conditions, 2 μL of each compound was added to columns 3 through 10 at the following final concentrations: 10 μM, 5 μM, 1 μM, 0.5 μM, 0.1 μM, 0.05 μM, 0.01 μM, and 0.005 μM. Columns 1 and 12 served as a no treatment control, Column 2 contained DMSO and Column 10 contained bortezomib at a final concentration of 2 μM. 20 μL of Alamar Blue Reagent was added to each well for a final well volume of 200 μL. Plate readings were taken at 0, 24, 48 and 72 hours using a Perkin Elmer Wallac 1420 Multilabel Counter. For Br23C and JHH-227, plate readings were taken every 48 hours due to slow *in vitro* growth rates. Each plate contained 6 replicates and all values are normalized to the DMSO control. GraphPad Prism 5 was used to calculate IC_{50} values.

Matrix Combination Screens

These methods have been described previously (Griner et al.). For each cell line tested, a total of 1000 cells per well in 5 μL of media was dispensed using a Multidrop Combi dispenser (Thermo Fisher Scientific Inc., Waltham, MA) and a small cassette into barcoded 1536 solid bottom white Greiner One tissue culture treated plates (catalog # 789173-F). Standard Neurocult media supplemented with EGF, FGF and heparin was used (Stem Cell Technologies). For the generation of standard 11 point dose response curves the cells were plated, followed by the immediate pintool addition of 23 nL of control compound (bortezomib) and library compounds using a Kalypsys pintool. For pre-plated matrix plates, the cells were added directly to the plates immediately after

compounds were acoustically dispensed using an ATS-100 (EDC Biosystems, Fremont, CA). The plates were then covered with stainless steel cell culture Kalypsys lids and incubated at 37˚C with 5% CO_2 under 95 % humidity. For cell proliferation assays, the cells were incubated for 48 hours and then 3 μL of CellTiter Glo luminescent cell viability assay reagent (Promega) was added using a Bioraptor Flying Reagent Dispenser (Aurora Discovery-BD). The plates were then incubated for 15 minutes at room temperature. The signal was captured using a 10 second exposure with a ViewLux (Perkin Elmer) contacting a luminescent filter. For apoptosis assays, the cells were incubated at either 8 or 16 hours and then 3 μL of Caspase Glo 3/7 luminescent apoptosis assay reagent (Promega) was added using the same method described above. Relative luminescence units (RLU) for each well were normalized to the median RLUs from the DMSO control wells as 100% viability or 0% caspase activation, and median RLUs from the bortezomib control wells as 0% viability or 100% caspase activation.

Animal Drug Efficacy Studies

Animals were maintained using approved IUCUC protocols. Athymic nude mice anesthetized with a ketamine/xylazine mixture and were implanted with 500,000 Br23C cells intracranially using a sterotatic frame. Surgical incisions were sealed with staples. Seven days post implantation, animals were randomized then divided into three groups of five mice. Group 1 and 2 were treated Monday through Friday by oral gavage with either 75mg/kg of BIIB021 or 25mg/kg of Bardoxolone methyl. Bardoxolone methyl animals were treated with 15mg/kg later in the experiment due to toxicity. Group 3 control animals received vehicle (1:1:8 cremaphor EL: DMSO: PBS) by oral gavage.

For drug combination studies, 500,000 JHH-520 cells were implanted. Animals were randomized then separated two groups of five mice and two groups of four mice. Treatment began seven days post-implantation. Two groups of animals were treated Monday through Friday by oral gavage with 75mg/kg of GDC-0941 plus 75mg/kg of BIIB021 or 75mg/kg of GDC-0941 plus 10mg/kg of PD325901. One group of animals received GDC-0941 as in the other treatment groups plus 75μg/kg of Marizomib intravenously twice a week. One group of control animals received daily gavage of vehicle (0.5% CMC/0.2% Tween80 in water). All animals were weighed thrice weekly for the duration of the experiment. Animals were sacrificed upon signs of intracranial tumor burden and de-brained. Kaplan-Meier curves were created using GraphPad Prism.

3 Results

Clinical histories

Each GBM oncosphere cell line was derived from a patient tumor with a final diagnosis of a GBM or a GBM variant. The patient demographic, tumor type and location are listed in Table 2. The HSR-GBM1, also known as 20913, was the only cell line examined that was not generated by our lab. This cell line was a gift from Angelo Vescovi and was derived from a primary GBM (Galli et al.). The Br23C cell line was derived from a primary GBM and was first implanted as a xenograft into nude mice. This xenograft, named Br23X, was then used to derive the Br23C cell line.

All other cell lines were generated directly from patient tumors. The JHH-136, JHH-227, JHU-1016B, and JHH-520 cell lines were derived from primary GBM tumors.

These patients had received no previous therapy. The remaining cell lines were derived from rare GBM variant tumors. The JHH-68 cell line was derived from a recurrent glioblastoma that had transformed to a gliosarcoma following radiation and chemotherapy. The JHU-0879 cell line was derived from a primary GBM with primitive neuroectodermal tumor (PNET) features. The JHH-505 cell line was derived from a primary GBM with an oligodendrogliomal component. Neither the JHU-0879 or JHH-505 patient received any previous therapy.

Table 2. Patient Demographics

Cell Line	**Gender**	**Diagnosis**	**Location**	**Prior Therapy**	**Survival* (Months)**
HSR-GBM1	M	GBM	Unknown	Unknown	Unknown
Br23C	F	GBM	Unknown	None	0
JHU-0879	F	GBM, with PNET-like component	Left Parieto-occipital Lobe	None	11
JHH-68	M	Gliosarcoma	Right Frontal Lobe	XRT, TMZ, Enzastaurin + Bevacizumab, Carboplatinum, BCNU + Thalidomide	3
JHH-136	M	GBM	Right Frontal Lobe	None	17
JHH-227	M	GBM	Right Periatrial Lobe	None	Lost to follow-up 6 months after surgery
JHU-1016B	M	GBM	Right Temporal Lobe	None	18
JHH-505	M	GBM with oligo component	Right Parietal Lobe	None	Lost to follow-up 5 months after surgery
JHH-520	F	GBM	Right Frontal Lobe	None	Lost to follow-up 1 month after surgery

*: Survival calculated from date of tissue acquisition.
XRT: Radiotherapy
TMZ: Temozolomide

Cell line independence

The first step to ensure that each cell line was distinct and independent was to complete Short Tandem Repeat (STR) profiling on each line. STR profiling is based on the number of repeats at 10 sites within the genome and is critical to determine the signature for each cell line. Two non-glioma cell lines, HeLa and K562, were included as controls. The 20 markers within each STR profile of each cell line were compared to all other cell lines. Overlap of 80% or more between two cell lines was considered evidence that these cell lines were not unique. Overall, none of the cell lines showed significant overlap with each other and are therefore independent cell lines as shown in Table 3. There was minimal overlap between each cell line and control markers as well.

Table 3. STR marker overlap

	HSR-GBM1	Br23C	JHU-0879	JHH-68	JHH-136	JHH-227	JHU-1016B	JHH-505	JHH-520	HeLa	K562
HSR-GBM1	20	5	6	6	7	4	5	4	6		
Br23C	5	20	8	6	3	5	5	6	3		
JHU-0879	6	8	20	5	2	5	5	5	8	6	7
JHH-68	6	6	5	20	8	9	10	5	5	7	8
JHH-136	7	3	2	8	20	8	11	7	7	5	8
JHH-227	4	5	5	9	8	20	9	4	4	4	8
JHU-1016B	5	5	5	10	11	9	20	9	7	5	7
JHH-505	4	6	5	5	7	4	9	20	9	6	7
JHH-520	6	3	8	5	7	4	7	9	20	6	6
HeLa			6	7	5	4	5	6	6	20	8
K562			7	8	8	8	7	7	6	8	20

In vivo tumor formation

The major criteria necessary for these cell lines to be useful for therapeutic testing was their ability to form tumors *in vivo*. Immunocompromised mice were injected intracranially with cells and each mouse was monitored for weight loss and signs of neurological defects. Upon death of the animal, the brain was extracted and preserved in formalin. Tissue was then cut and fixed on slides and H&E staining was done. Presence or absence of GBM histological features was assessed by a neuropathologist. Samples derived from GBM variants were compared to the primary tumor to determine if GBM variant features were present in the xenograft.

The *in vivo* tumor formation abilities of HSR-GBM1 and Br23C cell lines have been published previously (Galli et al.; Siu et al.; Bai et al.) (Joshi et al.). Of the remaining cell lines, all formed tumors *in vivo* except for JHH-68. A single animal died 676 days following implantation, but the brain was negative for tumor. All cell lines showed invasion along white matter tracts however JHU-0879 was the only cell line to form a compact mass with minimal invasion (Figure 3A-C). All cell lines showed histological features that define GBM such as mitotic figures (Figure 3D), areas of necrosis (Figure 3E) and vascular proliferation (Figure 3F). The level of invasion within the cell lines examined was greater than previous reports in other animal models (Bakir et al.; Di Tomaso et al.). Additional histological features of GBM were also present such as invasion (Figure 3G), satellitosis (Figure 3H) and subpial tumor spread (Figure 3I). The cell line establishment criteria are listed in Table 4.

Three of the cell lines were derived from variants of GBM containing unusual histologic features. JHH-68, a gliosarcoma, was unable to be analyzed due to the inability of the cell line to form tumors when implanted intracrainally. JHH-505 was isolated from a GBM with an oligodendroglioma component (GBM-O). In addition to hypercellularity and neovascularization common in GBM (Figure 4A), this primary tumor contained many small, round, regular cells with surrounding clear halos indicative of oligodendroglial differentiation (Figure 4B). The JHH-505 xenograft tumor retained features of a mixed GBM, with a dominant astrocytic component (Figure 4C) but also numerous scattered oligodendroglial cells that were prominent in some areas (Figure 4D). JHU-0879 was derived from a GBM with PNET features. The primary tumor contained areas of densely packed cells with scant cytoplasm and prominent nucleoli (Figure 4E). The xenograft contained these features as well but the nucleoli were more prominent in the xenograft than in the primary tumor (Figure 4F). Throughout both tumors were an abundance of mitotic and apoptotic cells. This data further validates the notion that oncosphere cell lines often recapitulate the histopathological features of the original patient tumor.

Table 4. Cell line establishment criteria.

Cell Line	**STR Profiling**	***In vivo tumor formation***	**# of cells injected/ Average survival (Days)**
HSR-GBM1	+	+ 4/4	$5x10^5$/58
Br23C	+	+ 10/10	$5x10^5$/48
JHU-0879	+	+ 1/3	$5x10^5$/87[a]
JHH-68	+	+ 0/3	$2.5x10^5$/676[a]
JHH-136	+	+ 3/3	$6x10^5$/161
JHH-227	+	+ 3/3	$2x10^5$/71
JHU-1016B	+	+ 4/4	$2.5x10^5$/194
JHH-505	+	+ 3/3	$5x10^5$/193
JHH-520	+	+ 2/2	$5x10^5$/84

STR: Short Tandem Repeat

[a]: The other two animals died but were unable to be evaluated for tumor formation

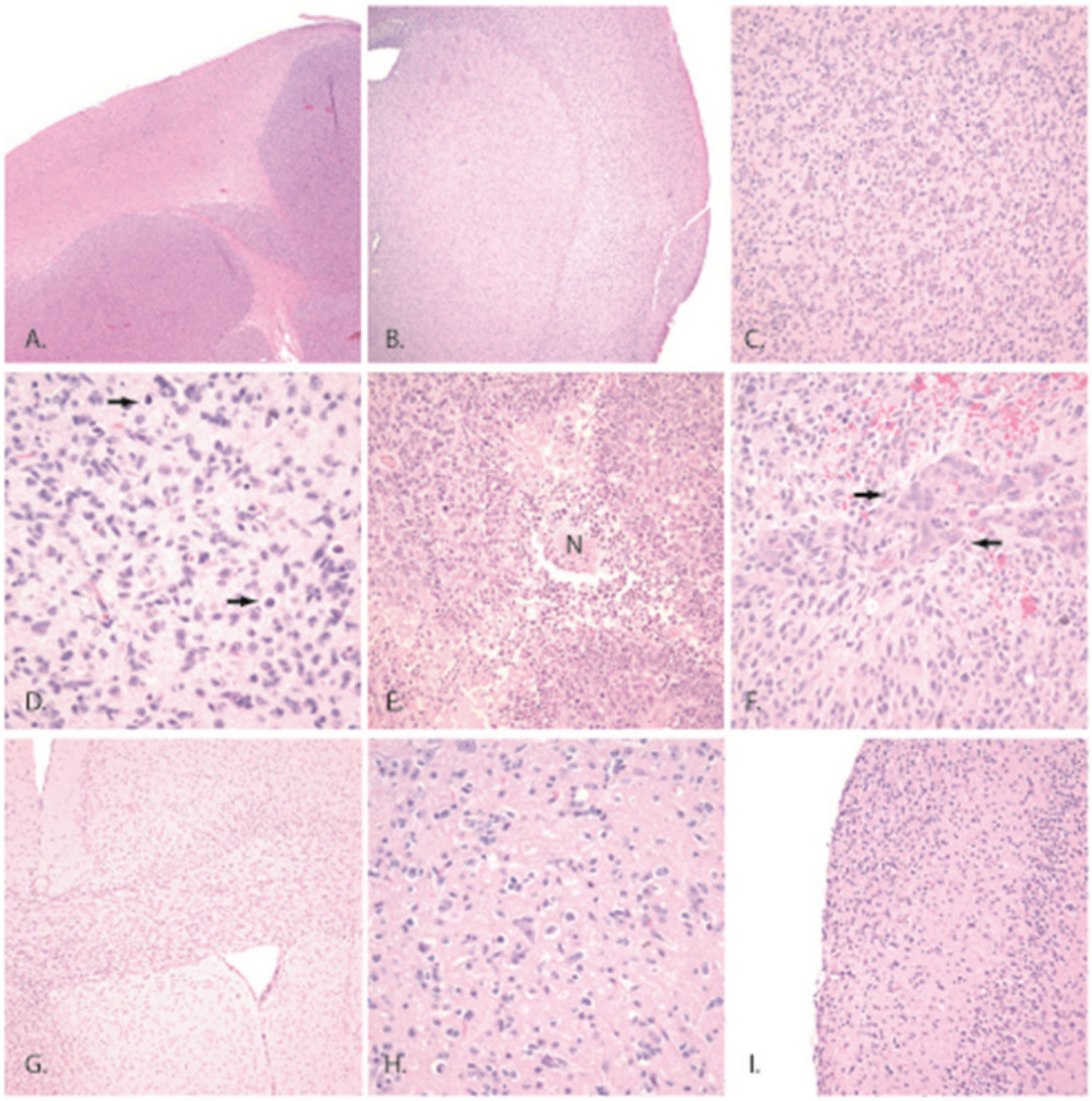

Figure 3. H&E stains of orthotopic tumors formed in athymic mice.

A, Only one of the 13 lines evaluated *in vivo* demonstrates compact, non-invasive growth patterns. B, The majority of lines showed diffuse invasion of normal parenchyma.
C, D, E, F hallmark features of glioblastoma were identified including increased mitotic activity, necrosis, and vascular proliferation. G, H, I Other histologic features specific to invasive gliomas, including spread through white matter tracts, neuronal satellitosis, and subpial tumor spread. Original magnification for panels A and B was 25x; for G and I, 50x; for C and E, 100x; and for D, F, and H, 200x.

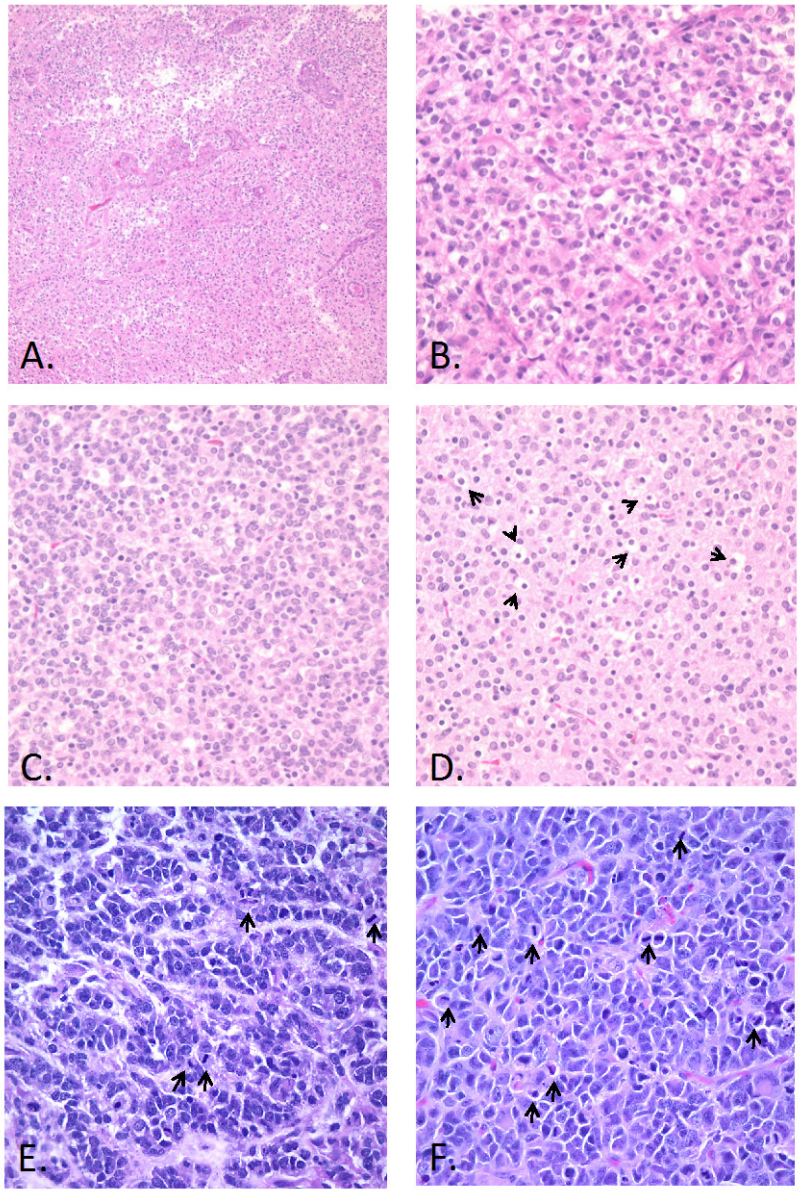

Figure 4. H&E stains of primary tumor tissue and orthotopic tumor from the GBM variant cell lines showing specific features of each variant.

A, B JHH-505 primary tumor has features of a GBM such as vascular proliferation and dense cellular areas and also areas of round, regular oligodendroglial cells.

C, D JHH-505 xenograft tumor has characteristics consistent with GBM-O.

E, F The JHU-0879 primary tumor and xenograft has areas consistent with PNET with hypercellularity containing cells with scant cytoplasm and prominent nucleoli. Arrows highlight mitotic or apoptotic cells. Magnification for panel A is 100X, panel B-F are 400X.

Each Oncosphere Cell Line has a Distinct Mutation Profile

Each oncosphere cell line was derived from a different patient tumor therefore, we explored deleterious point mutations and copy number alterations within each cell line. We began with the previously reported top glioblastoma candidate cancer (CAN) genes because these genes contain mutations that are drivers of glioblastoma cell growth (Parsons et al.). Table 5 shows the mutations present in all 10 CAN genes plus one additional oncogene, *c-MYC*. We explored additional oncogenes and tumor suppressor genes implicated as drivers in other cancer types but found very few alterations (Table 6). Presence or absence of PTEN and NF1 protein was verified by Western blot (Figure 5A and B).

Br23C, also called 060919, is slow growing *in vitro* but is notable due to its *in vivo* MST of 35 days (data not shown) and formation of brainstem tumors in rats when implanted into the pontine tegmentum (Siu et al.). An early xenograft from this tumor (Br23X) was sequenced previously (Parsons et al.). We compared the point mutations found in Br23X to the point mutations found in Br23C at passage 35 in order to estimate the amount of genetic drift that occurred over time. Br23X contained 32 missense mutations, found in the previous genomic assessment. Of these 32 mutations, 12 of them are identical to mutations found in Br23C (Table 8). The additional 22 missense mutations present in Br23X that were not found in Br23C could be due to differences in normalized controls, genome build differences or other differences in sequencing analysis.

The CAN gene mutations present in Br23C are a homozygous deletion of *PTEN*, a large focal gain of *c-MYC*, and homozygous point mutations in *NF1*, *TP53* and *RB1* paired with a heterozygous deletion of *RB1*. The *NF1* and *TP53* point mutations in

Br23C are identical to the point mutations found in Br23X. The *NF1* mutation is located at a donor splice site and is predicted to cause an increase in the inclusion of this exon. The loss of PTEN protein and presence of small amounts of NF1 protein was consistent with the genomic data (Figure 5A and B). The focal gain in *c-MYC* and the *RB1* mutation was not detected in Br23X. The *RB1* point mutation causes a premature stop codon, which results in the loss of 91 amino acids at the C terminus. The lost region contains the nuclear localization signal, critical phosphorylation sites and functional domains required for RB1 interactions with E4F1. This mutation is also predicted to cause nonsense mediated mRNA decay of *RB1* that would be highly deleterious since the second copy of *RB1* is deleted. This is a classic LOH event that occurred sometime between the xenograft acquisition and passage 35 of Br23C. This data shows that genetic drift does occur over time in oncosphere cell lines. The genomic profile of this cell line is most consistent with Mesenchymal GBM due to the *RB1* and *TP53* mutations.

HSR-GBM1 is fast growing *in vitro* and has an *in vivo* MST of 73 days (data not shown). This cell line contains a large focal gain of EGFR and deleterious point mutations in *CDKN2A*, *TP53*, *NF1* and PIK3R1. Interestingly, these point mutations in HSR-GBM1 are heterozygous with no loss of the normal allele so the effect of these mutations on overall cell function would be minimal. PTEN protein presence was consistent with the genomic data, however no NF1 protein was detected which is contradictory to the sequencing data (Figure 5A and B). HSR-GBM1 closely meets the criteria for Mesenchymal GBM due to the presence of *NF1* and TP53 mutations, however presence of a wild type *PTEN* and EGFR amplification were conflicting with the Mesenchymal subtype. This mixed genomic signature maybe due to early contamination

of this cell line with other GBM oncosphere cell lines. Further gene expression studies should be done to determine the GBM subtype of this cell line.

JHU-0879 was derived from a GBM with primitive neuroectodermal tumor (PNET) features and is fast growing *in vitro*. The *in vivo* tumor formation of this cell line has not been verified. JHU-0879 contains a heterozygous deletion of *PTEN* and homozygous point mutations in *PTEN* and *RB1*. The PTEN mutation is in the phosphatase tensin domain at a highly conserved residue and is predicted to cause an additional splice site which could result in loss of downstream exons. This mutation paired with the loss of one copy of *PTEN* is a classic LOH event however PTEN protein is present despite the mutation (Figure 5A). The *RB1* mutation results in a premature stop codon that eliminates the last 251 amino acids. This lost region contains the nuclear localization signal and many of the functional sites and domains of *RB1*. NF1 protein is present in the cell line (Figure 5B). Interestingly, JHU-0879 also has a large focal gain of *c-Myc*, which is common in GBM with PNET features (Perry et al.). The amplification of *c-Myc* is an indicator that our oncosphere cell line is able to retain genomic mutations common in the primary tumor tissue.

JHH-68 is slow growing cell line that was derived from a gliosarcoma and contains a homozygous deletion of *CDKN2A* and *PTEN*. JHH-68 also contains a point mutation in *TP53* at a highly conserved residue in the DNA binding domain. It is predicted to cause a novel alternative splice site which could result in a loss of downstream functional sites and domains. No PTEN protein is detectable in this cell line, however NF1 is intact (Figure 5A and B) which is consistent with the sequencing results. The *in vivo* tumor establishment of this cell line has not been determined. Gliosarcomas

are a rare tumor type which have a genomic profile similar to GBMs (Actor et al.) so our data correlates well with previous studies. Interestingly, this cell line is the only one that does not form tumors when implanted *in vivo* so this profile may be useful in determining the necessary mutations needed to form tumors.

JHH-136 is a fast growing cell line that was derived from a GBM. The *in vivo* MST of JHH-136 is 161 days (data not shown). This cell line only contains alterations in two CAN genes: a homozygous deletion of *CDKN2A* and *PTEN*. Consistent with the sequencing results, there is no detectable PTEN protein in this cell line, however NF1 protein is present (Figure 5A and B). Due to the lack of alterations in CAN genes such as *NF1* or *TP53*, this cell line was unable to be classified as a GBM subtype.

JHH-227 is slow growing cell line that was derived from a GBM with an *in vivo* MST of 73 days. This cell line contains a large focal gain of *EGFR*, a homozygous deletion of *CDKN2A* and an LOH event in *PTEN*. The *PTEN* mutation in JHH-227 results in alterations of the last 25 amino acids of PTEN where many phosphorylation sites and the PDZ domain are located. This mutation also results in the loss of the original stop codon and the addition of 10 amino acids on to the C terminus of PTEN. The functional impact this new mutation would have on PTEN is unknown but it is possible that PTEN may have increased activity due to the loss of the phosphorylation sites on the C terminus, which are critical to keeping PTEN in an inactive state. No PTEN protein was detectable in this cell line, however this may be due to the antibody being unable to bind to the mutated C terminus (Figure 5A). NF1 protein is present which is consistent with the sequencing data (Figure 5B). JHH-227 closely meets the criteria for Classical GBM due to the presence of an *EGFR* amplification and loss of *PTEN*.

JHU-1016B was derived from a GBM and grows fast *in vitro*. *In vivo*, the MST for this cell line is 194 days. This fast growing cell line contains a homozygous deletion of *CDKN2A*, an LOH event for *PTEN*, and a heterozygous mutation in *NF1*. The *PTEN* mutation in this cell line, C124W, is in the phosphatase tensin domain at a site, which is critical to PTEN function. In the early studies attempting to determine PTEN function, a dominant negative mutant with a C124S mutation was widely used due to its total loss of phosphatase activity (Tamura). The C124 site has also been shown to be oxidized by reactive oxygen species to form a disulfide bond with Cys71 to keep PTEN in an inactive conformation (S.-R. Lee et al.). This function would be lost as well since the new amino acid at this position is a tryptophan, which cannot be oxidized. However, all other domains of PTEN are normal so certain PTEN functions may be unaffected by this mutation. The heterozygous deletion of the second copy of *PTEN* leaves only the C124W PTEN to be active in JHU-1016B. The point mutation in *NF1* should have minimal effect on cell function due to the presence of a wild type *NF1*. PTEN protein and NF1 protein are detectable in this cell line despite the mutations in both genes (Figure 5A and 1B). This data is consistent with the sequencing results. JHU-1016B meets the criteria for Mesenchymal GBM due to the presence of an *NF1* mutation and a no loss of PTEN.

JHH-505 was derived from a GBM with an oliogodendroglioma component (GBM-O) and is a slow growing cell line *in vitro*. This is a rare and newly designated GBM subtype and this cell line forms tumors with histological characteristics of GBM-O. Examination of CAN gene alterations revealed only a homozygous deletion of *CDKN2A*. Some CAN genes had low level amplifications or heterozygous deletions but nothing

predicted to greatly affect cell function. Overall, this cell line contains numerous small copy number variation events on all chromosomes. We were unable to determine if PTEN or NF1 protein was present due to slow growth of this cell line. Further analysis must be done to determine the full extent of chromosomal loss and gains in JHH-505.

JHH-520 is a fast growing cell line derived from a GBM. The CAN gene mutations present in this cell line are a homozygous point mutation in *TP53* and homozygous deletion of *CDKN2A* and *NF1*. The point mutation in *TP53* is in the DNA binding domain. Another point mutation at this site has been previously reported in pancreatic adenocarcinoma of a patient with Li-Fraumeni syndrome (Lefrou et al.) . The H179Y mutation in the Li-Fraumeni patient was predicted to cause a complete loss of p53 function due to the loss of stability in the DNA binding loop. Although the JHH-520 p53 mutation is not the same amino acid change as the Li-Fraumeni mutation, the effect on protein function could be similar since a positively charged Histidine is altered to a negatively charged Aspartic acid. No PTEN protein was detectable in this cell line which was surprising due to the sequencing data showing no alteration in PTEN (Figure 5A). PTEN could be inactivated due to methylation changes or other mechanisms. No NF1 protein was present which is consistent with the sequencing data (Figure 5B).

We also compared our data to previous GBM sequencing efforts that utilized primary tissue. Overall, our genetic alteration frequencies are similar to previous studies with the biggest differences in the *NF1* and *EGFR* (Table 9). Finally, we examined the effect these alterations may have on individual signaling pathways. The pathways shown to be critical for GBM cell growth are the RB1, TP53, RAS, and the PI3K pathway (Parsons et al.; McLendon et al.). For this analysis, we excluded alterations that occurred

with a wild type copy present as the effect on pathway function was predicted to be minimal in these cases. In the cases where the protein expression was contradictory to the sequencing data, the protein absence overruled the sequencing data. JHH-505 was excluded from this analysis due to the lack of protein expression data. Table 7 shows all the alterations that involved homozygous deletions, amplifications, and heterozygous mutations paired with heterozygous deletions or loss of protein expression regardless of genomic information. PIK3 pathway alteration paired with RB1 pathway alteration was the most common combination. Taken together, this data shows that our oncosphere cell line panel contains GBM and rare GBM subtypes and that each cell line has a diverse genetic alteration profile. This information paired with the ability of many of these cell line to form tumors intracranially makes them a superior preclinical model for testing of new GBM therapeutics.

Table 5. Oncosphere Cell Line CAN gene alterations

	JHH-505	**JHU-1016B**	**Br23C**	**JHU-0879**	**JHH-136**	**JHH-68**	**JHH-520**	**HSR-GBM1**	**JHH-227**
CDKN2A	Hom Del	Hom Del			Hom Del	Hom Del	Hom Del	WT/ D74Pfs*45	Hom Del
TP53			C176F/ C176F			G244S/ G244S	H179D/ H179D	WT/ L130I	
EGFR								16 copies	16 copies
PTEN		Del/ C124W	Hom Del	Del/ K66E	Hom Del	Hom Del			Del/ R378I
NF1		WT/ L1153Tfs*42	I526S/ I526S				Hom Del	WT/ A1676T	
CDK4									
RB1			Del/ E837Gfs*2	S671Ffs*8/ S671Ffs*8					
IDH1									
PIK3CA									
PIK3R1								WT/ F156L, Q157del, E158del	
MYC			14 copies	18 copies					

Hom Del is homozygous deletion
WT/mutation is a normal allele paired with a heterozygous missense mutation
Del/mutation is a heterozygous deletion paired with a homozygous missense mutation

Table 6. Oncosphere and Tumor Suppressor Genes Examined

Gene Symbol	Oncosphere Cell Line Mutational Status
APC	None
BRAF	None
BRCA1	None
BRCA2	None
CTNNB1	None
ERBB2	None
HRAS	None
FLT3	None
KIT	None
KRAS	JHH-520: WT/M75I
MAP2K4	None
MET	None
NRAS	JHH-68: WT/T74I
PDGFRA	None
RET	None
SMAD4	None
STK11	None
VHL	None

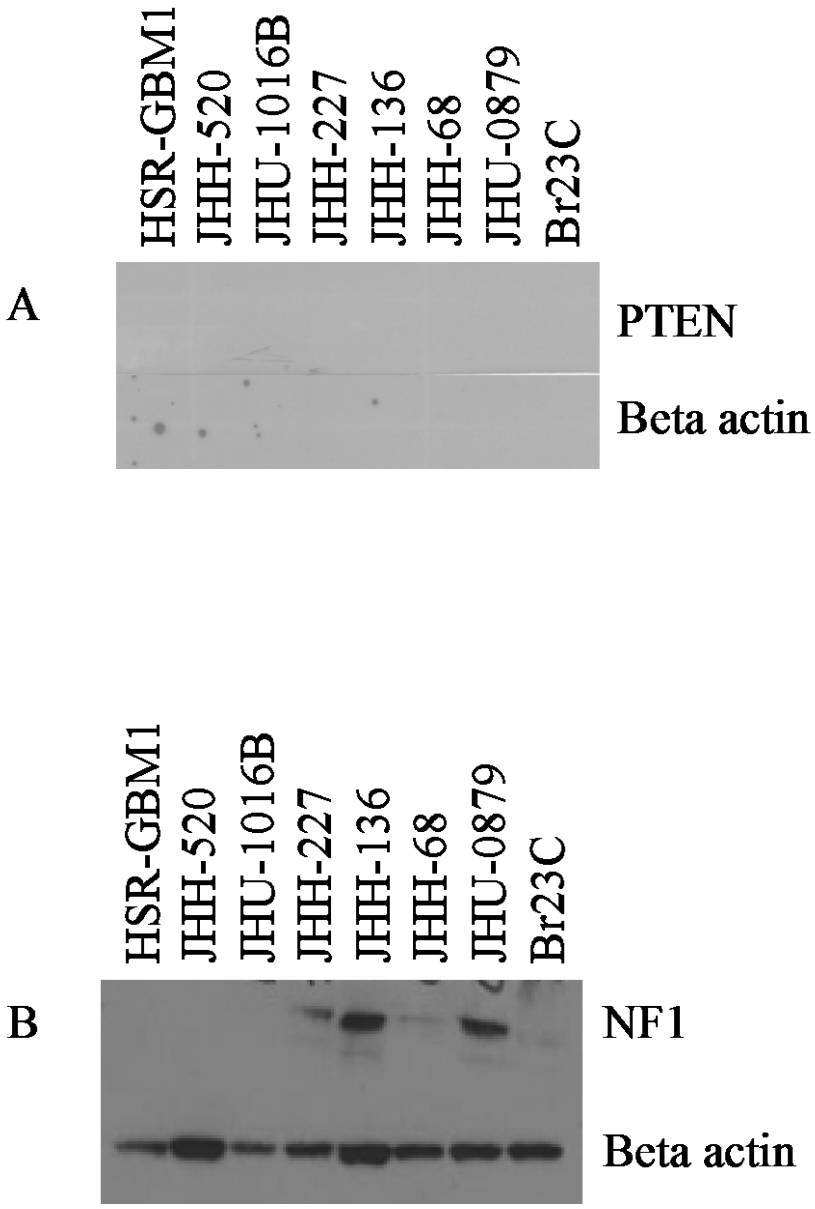

Figure 5 - Verification of sequencing data by Western blot

A. PTEN protein in eight oncosphere cell lines
B. NF1 protein in eight oncosphere cell lines

Table 7. Oncosphere Critical Pathway mutations.

Pathway Genes	JHU-1016B	Br23 C	JHU-0879	JHH-136	JHH-68	JHH-520	HSR-GBM1	JHH-227	Total
TP53/ MDM2/ MDM4		*TP53* mut			*TP53* mut	*TP53* mut			37%
EGFR							*EGFR* amp	*EGFR* amp	25%
PTEN/ PIK3CA/ PIK3R1/ IRS1	*PTEN* Mut, PP	*PTEN* Del, NP	*PTEN* Mut, PP	*PTEN* Del, NP	*PTEN* Del, NP	*PTEN* NP		*PTEN* Mut, NP	87%
NF1/RAS	*NF1*, NP	*NF1* Mut, PP				*NF1* Del, NP	*NF1*, NP		50%
RB1/ CDK4/ CDKN2A	*CDKN2A*	*RB1*	*RB1*	*CDKN2A*	*CDKN2A*	*CDKN2A*		*CDKN2A*	87%

Mut, mutated; Amp, amplified; Del, deleted; PP, protein present; NP, no protein.

Table 8. Genetic Alterations present in Br23C and Br23X

Gene Name	Amino Acid Change
GPR85	T352P
HIVEP1	F1388L
DIMT1L	E85K
LMX1A	C26Y
MPZ	Y187C
NF1	I526S
PDIA2	R303C
SLC9A2	R160H
SNRPA	G99D
TACC3	E680K
TNMD	D167Y
TP53	C176F
PTEN	Homozygous Deletion

Table 9. Comparison of Oncosphere Panel to Previous Studies

GBM CAN Genes	+Parsons et al, 2008	^TCGA, 2008	*Wilson et al, 2014
CDKN2A	50%	52%	66%
TP53	40%	35%	44%
EGFR	37%	45%	22%
PTEN	30%	36%	66%
NF1	15%	18%	44%
CDK4	14%	18%	0%
RB1	12%	11%	22%
IDH1	11%	ND	0%
PIK3CA	10%	15%*	0%
PIK3R1	8%	15%*	11%

+ Only heterozygous and homozygous point mutations, homozygous deletions and amplifications greater than 12 copies were counted.

^ Only heterozygous and homozygous point mutations, homozygous deletions and amplifications greater than 5.65 copies were counted.

*Only heterozygous and homozygous point mutations, homozygous deletions, and amplifications greater than 10 copies were counted.

Oncosphere cell lines show differential susceptibility to drug classes

We completed a quantitative high throughput drug screen using two GBM oncosphere cell lines. JHH-136 and JHU-1016B were selected due to their similar growth rates *in vitro* (data not shown). Both cell lines have a homozygous deletion of *CDKN2A,* which should result in uncontrolled cell division. The genomic profile differs between the cell lines in their PTEN and *NF1* alterations. JHH-136 has a total loss of PTEN protein due to a homozygous deletion and a wild type NF1 protein is present. JHU-1016B contains a phosphatase dead mutant PTEN protein and the NF1 protein is absent. This should result in both cell lines having constitutive PIK3 signaling however the non-phosphatase activity of PTEN should be normal in JHU-1016B. The loss of *NF1* in JHU-1016B should cause overactive signaling through the Ras pathway, while JHH-136 has normal Ras signaling. Additionally, both cell lines have a low level amplification of *EGFR* with three or four copies total.

Both cell lines were screened using the National Center for Advancing Therapeutics (NCATS) MIPE Oncology Collection 3.0, a 466 compound library containing compounds that are in various pre-clinical and clinical development, or have already been FDA approved. The strength of the MIPE Oncology Collection is the redundancy of drug classes within the library. For each drug target or mechanism of action, there are at least two different drugs in the MIPE within that class. Assays were done using 500 and 1000 cells per well and all compounds were tested in a 11-point dose responses. Active compounds were assessed as described previously, by first examining the % viability at each concentration tested (Mathews et al.). The % viability represents the percentage of live cells at all tested concentrations normalized to DMSO controls.

The maximum response, which is the % viability at the maximum concentration of compound tested, is a measure of the cytotoxic effect of a compound.

The correlation of the maximum responses for each compound on JHH-136 and JHU-1016B shows a strong positive correlation (R^2 = 0.80 and 0.85), which indicates that the number of cells used does not greatly affect the results of the screen and that the overall cytotoxic effect of the compounds is similar in both cell lines (Figure 7A and 2B). A hierarchical clustering of all maximum response values for each compound tested is show in Figure 7C. Comparison of the group means for the maximum response values for both cell lines using a two-tailed t-test shows minimal differences between JHH-136 and JHU-1016B (Figure 7D). The selection of cytotoxic compounds was based on a maximum response less than 30%, meaning that 70% of cells were killed at the maximum concentration tested. Next, all drugs were sorted using the Curve Response Class (CRC) classification, as previously described (Inglese et al.). Any compound with a CRC value of -1.1, -1.2, - 2.1 and -2.2 were considered high quality hits as these CRC values indicates a dose response with a minimum of 80% efficacy and an r^2 value of greater than 0.9. Any compounds with an alternative CRC value were considered inactive or inconclusive. There was no significant difference in the number of compounds within each CRC between JHH-136 and JHU-1016B (Figure 7E).

There were 52 compounds that were actives that in both JHH-136 and JHU-1016B using the maximum response criteria explained above (Table 10). Overall, the maximum response values for JHH-136 hits and JHU-1016B hits had similar group means (Figure 8A). Comparison of matched maximum response rates for each drug in both cell lines shows that overall most drugs have similar efficacy in both cell lines

(Figure 8B). Drug targets that were overrepresented in the list of actives by maximum response, in both cell lines, were EGFR inhibitors, NF-κB inhibitors, epigenetic modulators and apoptosis pathway inhibitors. EGFR inhibitors overall were more effective and had lower IC50 values in JHH-136 than JHU-1016B (Figure 8C and D). JHH-136 has only increased PIK3 signaling so in this cell line EGFR inhibition may be more effective. NF-κB inhibitors showed similar dose response curves and therefore similar IC50 values in both cell lines (Figure 8E and F). Apoptosis activators showed a pattern of dose response in JHH-136 that indicates that this cell line is more resistant to cell killing by this mechanism than JHU-1016B (Figure 8G and H). This suggests that cell lines with less over active signaling pathways are more difficult to induce apoptosis in. Overall, this data shows that the mutational profile of a tumor can have determine the efficacy of some classes of drug inhibitors.

Next, we examined hits specific to either JHH-136 or JHU-1016B. There were 20 hits that were selective for JHH-136 based on the maximum response being smaller in JHH-136 and larger than 30% activity (Figure 9A). A total of 16 different drug mechanisms of action were represented in the JHH-136 specific hits with EGFR as the most common target (Table 11). Effective compounds in this class were Dacomitinib, Afatinib, Pelitinib, Lapatinib and AEE-788. Pelitinib is shown as a representative drug from this class with a very different dose response curve for JHH-136 and JHU-1016B (Figure 9B). Cladribine, an adenosine deaminase inhibitor, was found to have the same IC_{50} value in both cell lines. However, the JHH-136 curve is shifted downwards killing almost 100% of cells at concentrations greater than the IC_{50} value. Only 33% of cells are killed at concentrations above the IC_{50} in JHU-1016B (Figure 9C). The remaining JHH-

136 specific hits have varied mechanisms of actions however only one drug within each class was a hit. This data suggests that in a cell line with increased PIK3 signaling and normal Ras signaling, very few drug classes can slow cell growth.

JHU-1016B had 36 hits that were specific to that cell line (Figure 9A). A total of 23 different drug targets or mechanisms of action were represented in this list of actives (Table 12). The most overrepresented drug targets for JHU-1016B were VEGFR inhibitors. Hits in this class include Foretinib, Cediranib, Regorafenib, and Sorafenib. Regorafenib, and Sorafenib have very similar chemical structures and each one mainly inhibits VEGFR along with additional activity against PDGFR and Raf kinases. The dose response for Regorafenib is shown as a representative of the group (Figure 9D). Regorafenib is a fairly weak cytotoxic compound for both cell lines, but is able to inhibit less than 30% of cell growth in JHU-1016B but not in JHH-136 at the maximum dose tested. This data shows that inhibition of VEGFR is more effective at high concentrations in cell lines with increased PIK3 and Ras signaling.

Other drug targets that were overrepresented in the JHU-1016B selective hits. Dual PIK3/mTOR inhibitors were GDC-0980, GSK-2126458, and PF-0521384. GDC-0980 is shown as a representative of the trend of dual PIK3/mTOR inhibitors (Figure 9E). For JHU-1016B, GDC-0980 is more effective at higher concentrations than in JHH-136. Interestingly, GSK-2126458 was very effective at low concentrations in JHU-1016B while in JHH-136 only the highest concentrations tested were effective (Figure 9F). Inhibitors specific for PIK3 or mTOR, such as GDC-0941 and Torin-2 showed a dose response similar to GDC-0980. Another common drug target was Cdk or Chk inhibitors which block the ability of cells to enter mitosis. AT-7519 is shown as a representative of

this class of drugs (Figure 9G). High concentrations of this drug are effective in JHU-1016B but not in JHH-136. This data shows that these classes of drugs are effective at low concentrations in cells with a similar mutation profile to JHU-1016B. Taken together, this data shows that minimal genomic differences in cell lines can result in differing drug efficacy.

Figure 7 (next page). Results from quantitative high throughput screen

A. Correlation plot of maximum response between JHH-136 and JHU-1016B with 500 cells per well ($r^2 = 0.85$) normalized to DMSO only control.
B. Correlation plot of maximum response between JHH-136 and JHU-1016B with 1000 cells per well ($r^2 = 0.87$) normalized to DMSO only control.
C. Hierarchical clustering with Euclidean distance of maximum response in JHH-136 and JHU-1016B. Green represents an increase in maximum response, red represents a decrease and black represents no change in viability.
D. Maximum response values for all drugs tested in JHH-136 compared to JHU-1016B. The group means are marked with a red line. The means are not statistically significant as determined by a two-tailed t-test.
E. Curve response class (CRC) distribution for all compounds tested. CRC classes -1.1, -1.2, -2.1, and -2.2 were considered active. CRC classes -1.3, -1.4, -2.3, -2.4 were considered inconclusive. CRC class -4 was considered inactive.

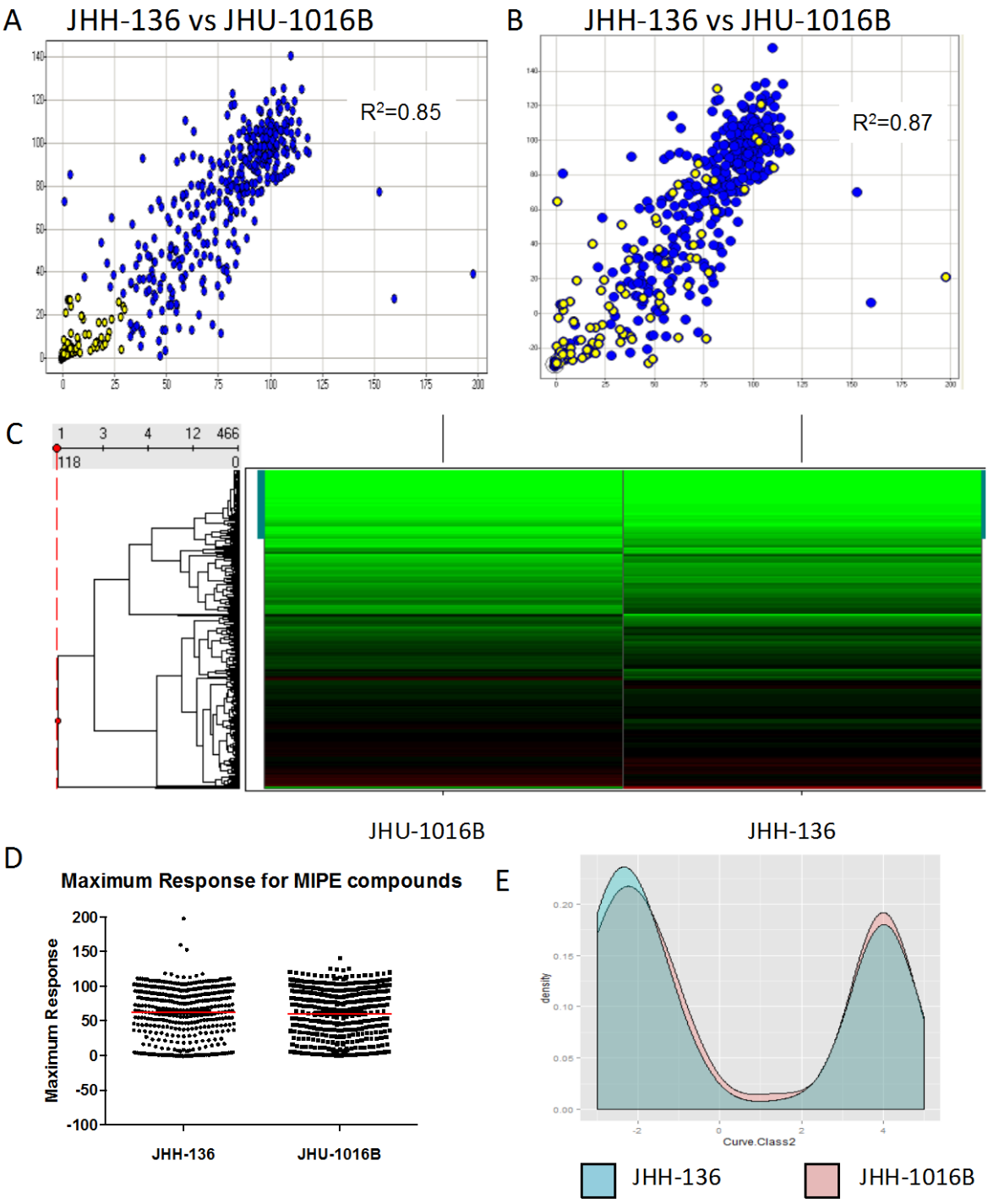
A
JHH-136 vs JHU-1016B
R²=0.85
B
JHH-136 vs JHU-1016B
R²=0.87
C
1
3
4
12
466
118
0
JHU-1016B
JHH-136
D
Maximum Response for MIPE compounds
Maximum Response
200
150
100
50
0
-50
-100
JHH-136
JHU-1016B
E
density
0.20
0.15
0.10
0.05
0.00
-2
0
2
4
Curve.Class2
JHH-136
JHU-1016B

Figure 8 (next page) - Figure 3. Dose responses from pan-actives

A. Maximum response values for 52 actives in both JHH-136 and JHU-1016B. The group means are not significant as determined by a student's unpaired t-test.
B. Maximum response values for the 52 actives for both cell lines were matched. The red dots are the maximum response of a compound in JHH-136 and the blue dot is the maximum response of the same compound in JHU-1016B as shown by the connecting line. The differences are not significant as determined by two way ANOVA analysis.
C. Dose response curves of AV-412, NGCG182713, WZ-4002, CUDC-101 and Vandetanib in JHH-136.
D. Dose response curves of AV-412, NGCG182713, WZ-4002, CUDC-101 and Vandetanib in JHU-1016B.
E. Dose response curves of CDDO-Me, Withaferin A, NGCG161703-2, and IMD-0354 in JHH-136.
F. Dose response curves of CDDO-Me, Withaferin A, NGCG161703-2, and IMD-0354 in JHH-1016B.
G. Dose response curves for Gossypol, Navitoclax, Obatoclax, TW-37, PAC1 and YM155 in JHH-136
H. Dose response curves for Gossypol, Navitoclax, Obatoclax, TW-37, PAC1 and YM155 in JHU-1016B

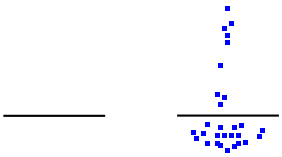

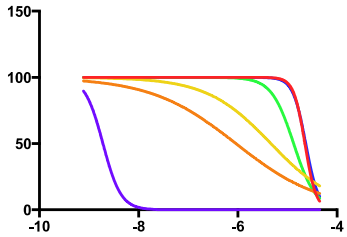
150
100
50
0
-10
-8
-6
-4

Table 10. Drug Hits for both JHH-136 and JHU-1016B

Drug Mechanism of Action	Compound Names
EFGR inhibitors	AV-412, Canertinib, WZ-4002, CUDC-101, Vandetanib^
NF-κB/IKK-beta inhibitors	Bardoxolone Methyl, Withaferin A, NCGC00161703-02, IMD-0354
Apoptosis Activators	Navitoclax, Obatoclax, Gossypol, PAC-1, TW-37, YM155
Epigenetic Modulators	Panobinostat, BIX-01294, Belinostat, Mocetinostat
Bcr-Abl inhibitor	Nilotinib^, Ponatinib^
JNK inhibitors	BI-78D3, SR-3306
PI3K inhibitors	Wortmannin, BAG956, CAY10626
BMPR/ALK inhibitors	LDN-193189, TAE684
JAK1/2 inhibitors	Lestaurtinib, Degrasyn
Chk1/Cdc25 inhibitor	AZD7762, NSC 663284
HSP90 inhibitor	BIIB021
FGFR inhibitors	Dovitinib
PKC inhibitor	Chelerythrine chloride
IDO inhibitor	CAY10581
cPEPCK inhibitor	NCGC00263130-01
Proteasome inhibitor	MLN-2238
Antibacterial/Anticoccidal	Salinomycin
Seletive Estrogen Receptor Modulator	Tamoxifen^
ERK inhibitor	NCGC00242487-01
Vitamin A acid analogue	Retinoic acid p-hydroxyanilide
PAR1 Receptor Agonist	SCH-79797
VEGFR inhibitor	Nintedanib
TAK1 inhibitor	NCGC00253463-01
Glucocorticoid Receptor Agonist	Cortivazol^
Plk inhibitor	BI-2536
DNA-PK inhibitor	Nu7441
Substance P agonist	Aprepitant^
Arteminisin analogue	Diartallox
Inducible T Cell Kinase inhibitor	NCGC00188382-02
Casein Kinase Inhibitor	Silmitasertib

^ drug is FDA approved

Figure 9 (below) - Active compounds selective for either JHH-136 or JHU-1016B

A. Venn diagram showing the number of actives in oncosphere cell line.
B. Dose response curves for Pelitinib, an EGFR inhibitor.
C. Dose response curves for Cladribine, an adenosine deaminase inhibitor.
D. Dose response curves Regorafenib, a VEGFR/PDGFR inhibitor.
E. Dose response curves for GDC-0980, a dual PIK3/mTOR inhibitor.
F. Dose response curves for GSK-2126458, a dual PIK3/mTOR inhibitor.
G. Dose response curves for AT-7519, a Cdk inhibitor.

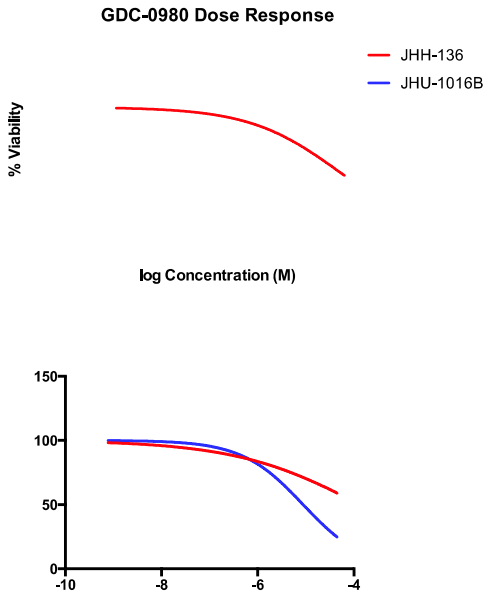
GDC-0980 Dose Response
JHH-136
JHU-1016B
% Viability
log Concentration (M)
150
100
50
0
-10
-8
-6
-4

Table 11. JHH-136 Specific Hits

Drug Mechanism of Action	**Compound Names**
EGFR inhibitors	Dacomitinib, Afatinib,^ Pelitinib, Lapatinib^, AEE-788
Adenosine Deaminase inhibitor	Cladribine^
NF-κB inhibitor	PS1145
Ribonucleotide Reductase inhibitor	Gemcitabine^
AKT inhibitor	MK-2206
PI3K inhibitor	CAY10626
mTOR inhibitor	Everolimus^
Pan-tyrosine kinase inhibitor	PD-166285
Flt3/Pim inhibitor	SGI-1776
CXCR1/2 receptor antagonist	PD-0220245
Antiviral	Efavirenz
MDM2 inhibitor	HLI-373989
Bruton's tyrosine kinase inhibitor	Ibrutinib
Retinoid, RAR-gamma agonist	CD437
DNMT inhibitor	5-azacytidine^
Non steroidal LXR agonist	GW 3965 hydrochloride
Topoisomerase II inhibitor	Topotecan hydrochloride^
Arteminisin analogue	NCGC00263270-01

^drug is FDA approved

Table 12. JHU-1016B Specific Hits

Drug Mechanism of Action	Drug Name
VEGFR inhibitors	Foretinib, Cedirinib, Sorafenib^, Regorafenib^
mTOR or PI3K or dual mTOR/PI3K inhibitors	GDC-0980, Torin-2, PF-0521384,GSK-2126458, GDC-0941,
Cdk/Chk inhibitor	AT7519, Selicicib, PF-477736
Hsp90/Hsp70 inhibitor	Alvespimycin hydrochloride, VER-155008
Proteasome Inhibitors	Bortezomib, Carfilzomib
TRPV4 antagonist	DE-096
c-MET inhibitor	AMG-51, Crizotinib^
HDAC Inhbitors	Romidepsin, AR-42
Raf kinase inhibitor	RAF-265
USP2 inhibitor	NCGC00262398-01
Vitamin analogue	1-alpha-Hydroxyergocalciferol
Jak2 inhibitor	NVP-BSK805
GR agonist	Deactyl Cortivazol
CAR agonist	CITCO
CFTR Channel Activator	Ivacaftor^
Lck Inhibitor	AMG-47a
DNA-PK Inhibitor	Ku0060648
Plk inhibitor	GSK-461364A
Trk inhibitor	AZ 23
Aurora kinase inhibitor	ENMD-981693
EGFR inhibitor	Gefitinib^
Monopolar spindle 1 inhibitor	AZ-3146
Wnt signaling Inhibitor	ICG-001
Tie2 inhibitor	AMG-Tie2-1

^drug is FDA approved

Hits were validated in additional oncosphere cell lines and tested *in vivo*

Three compounds were chosen from the list of compounds that were cytotoxic in both JHH-136 and JHU-1016B cells for further validation in six additional oncosphere cell lines. BIIB021, Bardoxolone methyl, and Obatoclax are all compounds that had similar IC_{50} values for both cell lines. BIIB021 and Bardoxolone methyl were effective in all cell lines tested at sub-micromolar concentrations and all dose response curves contained two asymptotes, as in the primary screen (Figure 10A-D). Obatoclax showed dissimilar IC_{50} values and dose response curves in all cell lines tested (Figure 10E-F). BIIB021 and Bardoxolone methyl were chosen for testing *in vivo* as single agents. Obatoclax was not tested due to a previous study showing a lack of single agent efficacy in an intracranial model of GBM (Cruickshanks et al.). Br23C cells were implanted intracranially and treatment was started seven days following implantation. BIIB021 (75mg/kg) and Bardoxolone methyl (25mg/kg) were administered once daily by oral gavage Monday through Friday. Control animals received vehicle by oral gavage. BIIB021 was well tolerated however it failed to increase MST (Figure 11A). Animals treated with Bardoxolone methyl experienced significant weight loss so treatment was stopped for a period of three days then restarted at a lower dose (15mg/kg). This treatment group had a lower MST than control animals due to toxicity (Figure 11B). Taken together, this data shows that the qHTS format was successful in determining effective *in vitro* compounds, however this data did not translate into *in vivo* extension of survival in the Br23C model.

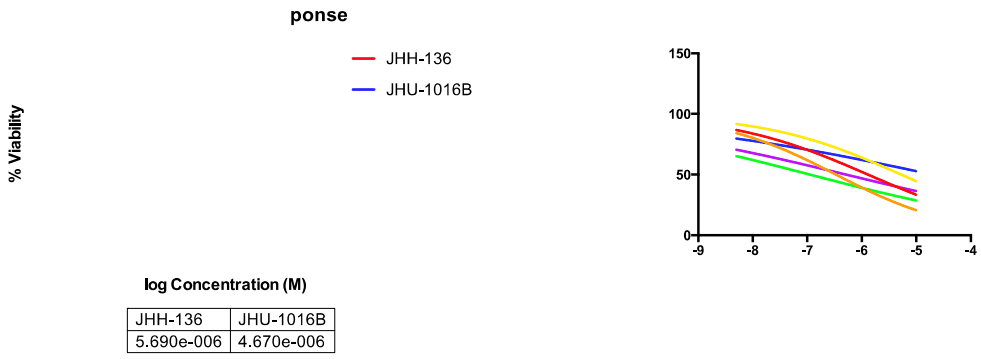

JHH-136	JHU-1016B
5.690e-006	4.670e-006

Figure 10. Hit validation and secondary screening

A. Dose response curves for BIIB021 from the primary screen using a qHTS format.
B. Dose response curves for BIIB021 in six oncosphere cell lines using non-qHTS format
C. Dose response curves for Bardoxolone methyl from the primary screen using a qHTS format.
D. Dose response curves for Bardoxolone methyl in six oncosphere cell lines using a qHTS format.
E. Dose response curves for Obatoclax from the primary screen using a qHTS format.
F. Dose response curves for Obatoclax in six oncosphere cell lines using a non-qHTS format.

A

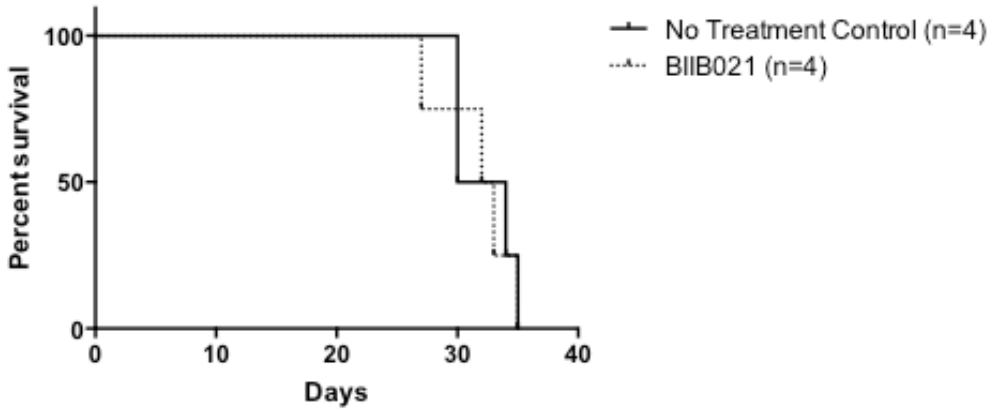

B

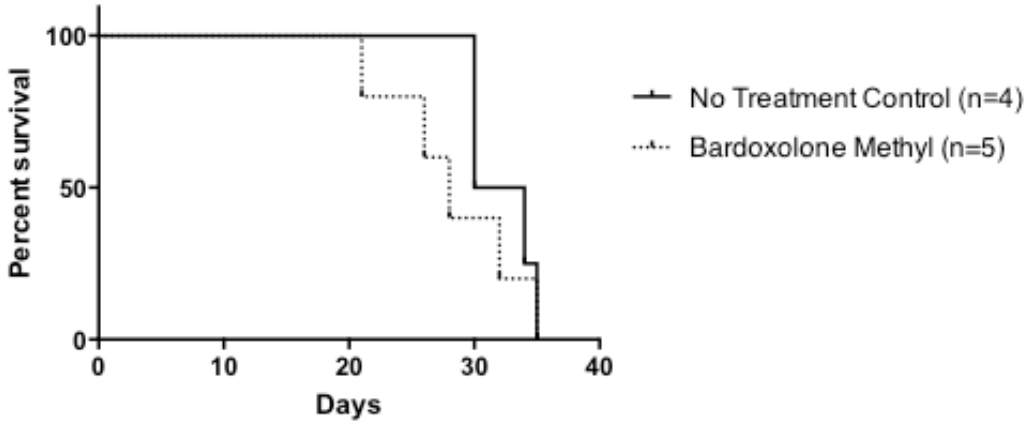

Figure 11 - BIIB021 and Bardoxolone methyl show no single agent efficacy *in vivo*

A. Kaplan Meier curve of the Br23C model treated with control or 75mg/kg of BIIB021.
B. Kaplan Meier curve of the Br23C model treated with control or 25mg/kg of Bardoxolone methyl.

Drug Combination Matrix

Due to the lack of success with single agents from the MIPE screen in our glioma models, we sought to determine if drug combinations would be a better strategy. We attempted to test Temozolomide in combination with compounds from the NINDS and Sigma-LOPAC drug libraries using a non-high throughput system in oncosphere cell lines. Temozolomide and drug library compounds were kept at fixed concentrations of 2μM and 4μM, respectively. Hits selected from this assay were then validated using a range of concentrations for both drugs to obtain the synergistic range. Issues encountered in this model were non-reproducibility of data and the short half-life of TMZ *in vitro* (Denny et al.). Additionally, the use of fixed concentrations of both drugs in screening resulted in elimination of possible synergistic combinations. Clearly, a better system for screening would allow for testing multiple concentrations of two drugs simultaneously to assess synergy.

A high throughput drug combination matrix screening system was developed to allow for screening of many compounds using a range of concentrations. First, we selected hits from our MIPE screen to be used in the drug combination matrix screen (Table 13). These 29 compounds were combined in an all versus all matrix, using 6 concentrations of both drugs. JHH-136 was used for the 6x6 matrix screen. 435 drug combinations were done with 29 compounds. Of these, 43 were chosen for an expanded 10x10 matrix using 10 concentrations of both drugs (Table 14). The 10x10 screen was done using JHH-136 and JHH-520. The data from these screens revealed interesting interactions between many drugs.

Table 13. Compound list of drugs used in the 6x6 all versus all matrix and the IC_{50} values obtained in the MIPE screen

Compound Name	Mechanism of Action/Target	JHH-136 (uM)	JHU-1016B (uM)
Carfilzomib	proteasome inhibitor	0.0007	0.1482
Ixazomib	proteasome inhibitor	0.0083	0.0132
Picropodophyllin	IGF-R inhibitor	0.0132	0.0662
Pelitinib	EGFR inhibitor	23.485	29.5659
CNF-2024	HSP90 inhibitor	0.0935	0.0833
TAK-733	MEK inhibitor	0.0662	0.0187
Trametinib	MEK inhibitor	0.0332	0.0083
Panobinostat	HDAC inhibitor	0.1663	0.2093
OSI-027	mTOR inhibitor	1.177	0.4686
GDC-0980	mTOR inhibitor	1.3207	0.5899
AZD-8055	mTOR inhibitor	0.0372	0.059
GSK 2126458	PIK3 inhibitor	14.818	0.0526
GDC-0941	PIK3 inhibitor	41.7629	1.6626
Flavopiridol	Cdk 1/2/4/6/7/9 inhibitor	0.0296	0.0743
Cladribine	Adenosine Deaminase Inhibitor	0.0762	0.0762
Doxorubicin	Topo II inhibitor	0.1321	0.1865
Topotecan HCl	Topo II inhibitor	5.8992	0.7427
Combretastatin A-4	Tubulin polymerization inhibitor	1.4818	0.0093
Plinabulin	Tubulin polymerization inhibitor	209.3103	0.3317
Mebendazole	Tubulin polymerization inhibitor	10	ND
retinoic acid p-hydroxyanilide	Vitamin A acid analogue	9.3495	23.485
Bardoxolone methyl	Nf-kB inhibitor	1.049	0.935
NCGC00161703	Nf-kB inhibitor	0.935	0.7427
PAC-1	Caspase 3 activator	20.931	20.931
Obatoclax	Bcl-xl inhibitor	6.619	3.7221
Dihyrdoartemisinin	Anti-malarial	ND	ND
Rotenone	Pesticide	ND	ND
SR-3306	JNK 1/2/3 inhibitor	0.0296	0.0743
JK 184	Shh/Gli1 inhibitor	2.9566	2.9566

Table 14. Drug combinations selected for 10x10 matrix

Drug Combinations		
Carfilzomib + Bardoxolone methyl	GSK-2126458 + Bardoxolone methyl	Trametinib + AZD-8055
Carfilzomib + Cladribine	GSK-2126458 + CNF-2024	Trametinib + CNF-2024
Carfilzomib + GSK-2126458	GSK-2126458 + Marizomib	Trametinib + Marizomib
Carfilzomib + PAC-1	GSK-2126458 + Navitoclax	Trametinib + Navitoclax
Carfilzomib + SR-3306	GSK-2126458 + PAC-1	Trametinib + PAC-1
Cladribine + AZD-8055	GSK-2126458 + Trametinib	Trametinib + Pelitinib
Cladribine + CNF-2024	Mebendazole + AZD-8055	Trametinib + SR-3306
Cladribine + GSK-2126458	Mebendazole + OSI-027	
Cladribine + Marizomib	Mebendazole + Navitoclax	
Cladribine + Mebendazole	Mebendazole + Pelitinib	Self Crosses:
Cladribine + Navitoclax	Obatoclax + AZD-8055	Cladribine
Cladibrine + Obatoclax	Obatoclax + CNF-2024	GSK-2126458
Cladribine + PAC-1	Obatoclax + GDC-0941	Mebendazole
Cladribine + Pelitinib	Obatoclax + Mebendazole	Obatoclax
Cladribine + Trametinib	Obatoclax + Pelitinib	Trametinib
GDC-0941 + CNF-2024	PAC-1 + CNF-2024	
GDC-0941 + Mebendazole	PAC-1 + SR-3306	

PI3K Inhibitors are synergistic in many drug combinations

GSK-2126458 is dual PI3K/mTOR inhibitor that has shown efficacy in animal models of breast cancer (Knight et al.). As a single agent, this compound had similar efficacy in JHH-136 and JHH-520 with a maximum response rate of approximately 40%. This compound showed synergy in combination with many compounds in the 10x10 screen for both JHH-136 and JHH-520. The most synergistic combinations were GSK-2126458 paired with either Marizomib or Trametinib (Figure 12). Marizomib, a proteasome inhibitor, is a very effective single agent drug in JHH-136 and JHH-520, killing 100% of cells. Combining Marizomib with GSK-2126458 lowered the concentration of Marizomib needed to kill 100% of cells. Carfilzomib, another proteasome inhibitor, had a similar downshift in the concentration needed to kill 100% of cells when combined with GSK-2126458. Trametinib, a MEK inhibitor, has similar efficacy to GSK-2126458 as a single agent yet the combination treatment causes 100% cell death. GSK-2126458 was also combined with CNF-2024, Navitoclax, PAC-1, and Bardoxolone methyl but little to no synergy was observed in these combinations. Overall, more synergy in these combinations were present in JHH-136 than JHH-520, however this effect was only at the highest concentrations of both drugs.

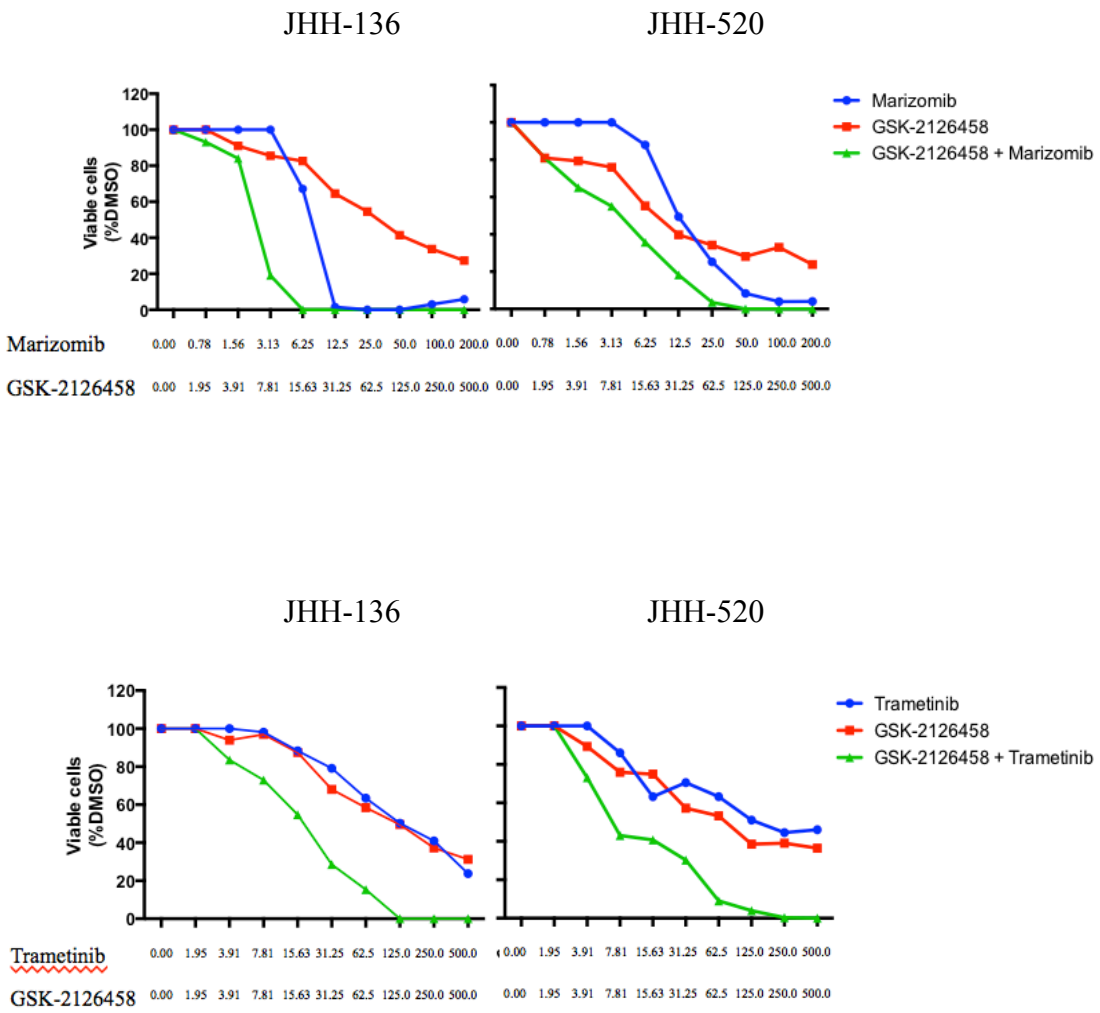

Figure 12. Most synergistic GSK-2126458 combinations.

Graph of inhibition in JHH-136 or JHH-520 cell treated with single agents or drug combination.

Trametinib and Cladribine drug combinations are more effective in JHH-136

Trametinib, an FDA approved MEK inhibitor, was also synergistic with many compounds (Figure 13). GSK-2126458, as discussed previously, was one of the most effective Trametinib combinations. AZD-8055, SR-3306 and Navitoclax were also very synergistic when combined with Trametinib in JHH-136. The synergy was not as defined for these same drug combinations in JHH-520. AZD-8055 is an mTOR inhibitor with a maximum response rate of approximately 60% as a single agent. In combination with Trametinib, 100% of cell death occurs at the highest concentrations in JHH-136. This combination was less efficacious in JHH-520. SR-3306, a JNK inhibitor, has similar single agent efficacy to Trametinib, but the combination of both drugs causes 100% cell death in JHH-136. In JHH-520, there is no difference in cell death in SR-3306 and Trametinib plus SR-3306. Another drug that was synergistic in combination with Trametinib was Navitoclax, a Bcl-xL and Bcl2 inhibitor. This drug combination was interesting due to the minimal activity of Navitoclax as a single agent in JHH-136 and JHH-520. Navitoclax in combination with Trametinib causes 100% cell death in JHH-136 but in JHH-520 the synergy is only present at the highest concentrations. Trametinib was also combined with CNF-2024, Pelitinib, and PAC-1. These combinations caused 30% or less viable cells but the efficacy was similar to single agent efficacy of one drug within the combination.

There was one compound with vastly different single agent activity in one of the two cell lines used for screening. Cladribine, an FDA approved adenosine deaminase inhibitor, causes cell death by damaging DNA. As a single agent, Cladribine has a maximum response rate of less than 10% in JHH-136. However in JHH-520, Cladribine

has a maximum response rate of 80%. Cladribine was combined with 11 drugs and the most effective combinations in JHH-136 were with GSK-2126458 and Pelitinib. Both these combinations caused lower concentrations of Cladribine to be more efficacious (Figure 14). For JHH-520, both combinations produce the same result as GSK-2126458 or Pelitinib as single agent. This data is consistent with the single agent drug screen which found that Cladribine was ineffective in JHU-1016B yet very efficacious in JHH-136. Other drug combinations in JHH-136 involving Cladribine caused minimal benefit over Cladribine alone.

Figure 13 (below). Combinations with Trametinib are synergistic.

Inhibition of JHH-136 and JHH-520 treated with single agent or drug combinations.

JHH-136 JHH-520

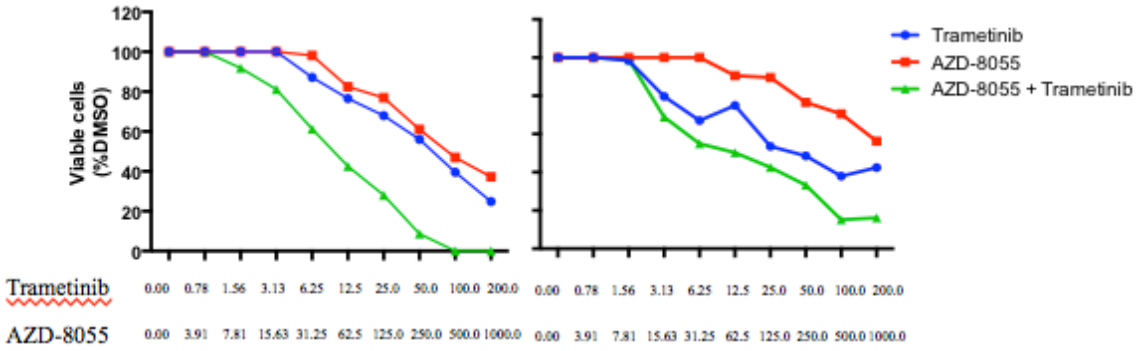

JHH-136 JHH-520

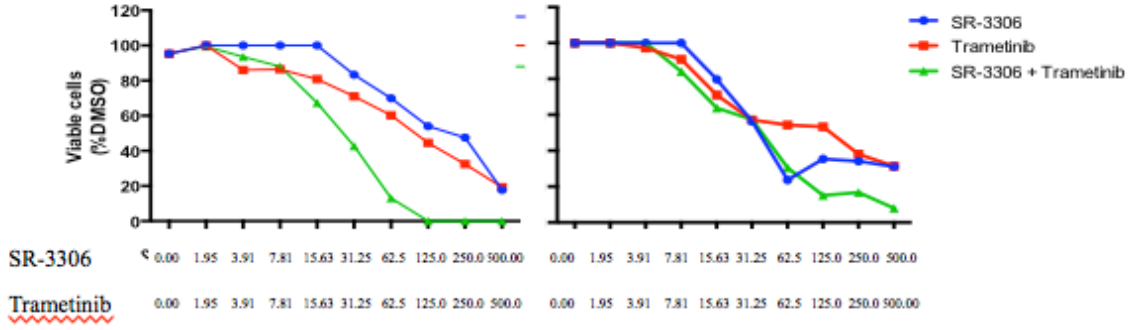

JHH-136 JHH-520

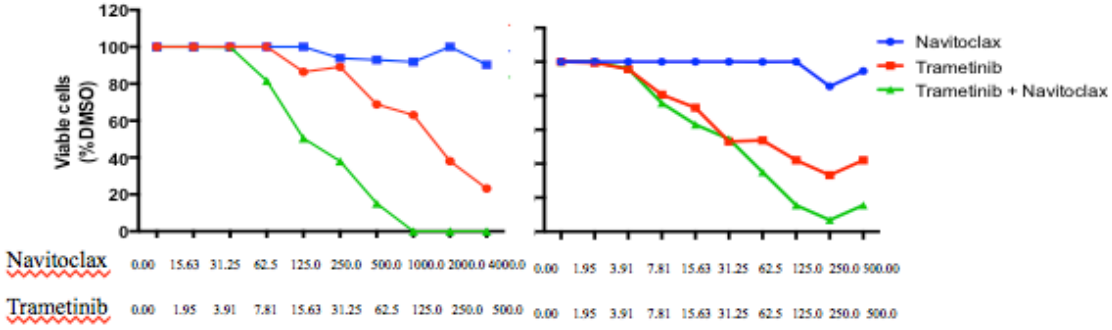

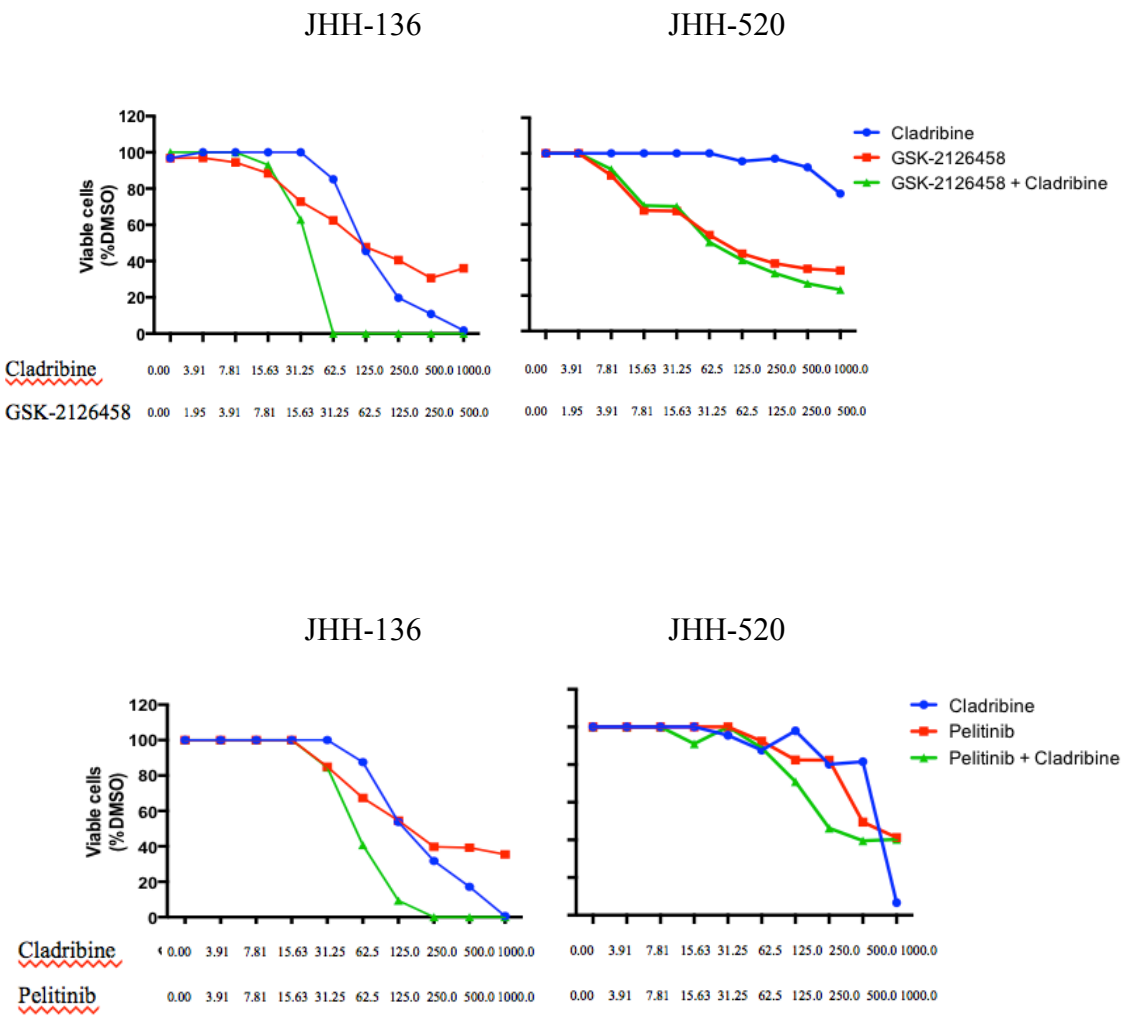

Figure 14. Cladribine combinations are only synergistic in JHH-136.

Inhibition of JHH-136 and JHH-520 treated with single agent or drug combinations.

Drug combinations involving compounds with single agent efficacy *in vivo* had minimal synergy

Drugs were also tested that our lab has evidence of single agent efficacy in GBM animal models. Mebendazole is an anti-helmenthic drug that was found to extend survival in mouse and rat models of glioma (Bai et al.). Mebendazole acts as a microtubule polymerization inhibitor, which has various anti-cancer mechanisms including the induction of apoptosis. *In vitro*, the IC_{50} of Mebendazole is higher in glioma stem cells than in adherent cell lines and the maximum response rate is 90% or greater in JHH-136 and JHH-520. Mebendazole was combined with Cladribine, Pelitinib, GDC-0941, Navitoclax, Obatoclax, AZD-8055, and OSI-027. Of these Navitoclax was the most synergistic in both cell lines, however this combination had a maximum response rate of 25-50% (Figure 15). As mentioned previously, Navitoclax as a single agent has minimal drug efficacy. All other combinations with Mebendazole, such as GDC-0941, had minimal difference in efficacy between the combination and the single agent. Mebendazole intracranial concentrations can reach 3 μM so this drug combination will require further exploration.

PAC-1 is a caspase 3 activator that extends survival in mouse and rat models of GBM. Caspase 3 levels are high in our oncosphere cell lines which correlates well with drug efficacy (Peterson et al.). As a single agent, PAC-1 had minimal activity in JHH-136 and JHH-520. PAC-1 was combined with Carfilzomib, SR-3306, GSK-2126458, Cladribine, CNF-2024 and Trametinib. The most synergistic of these combinations was Carfilzomib with PAC-1 in JHH-136 (Figure 15). This combination lowered the concentration of Carfilzomib needed to cause 100% cell death. This level of synergy was

not present in JHH-520. Other combinations with PAC-1, such as PAC-1 and GSK-2126458, failed to show even minimal synergy in either cell line. Further studies must be done to find compounds that are efficacious with PAC-1.

Figure 15 (below). Mebendazole and PAC-1 combinations were not synergistic Inhibition of JHH-136 and JHH-520 treated with single agent or drug combinations.

JHH-136 JHH-520

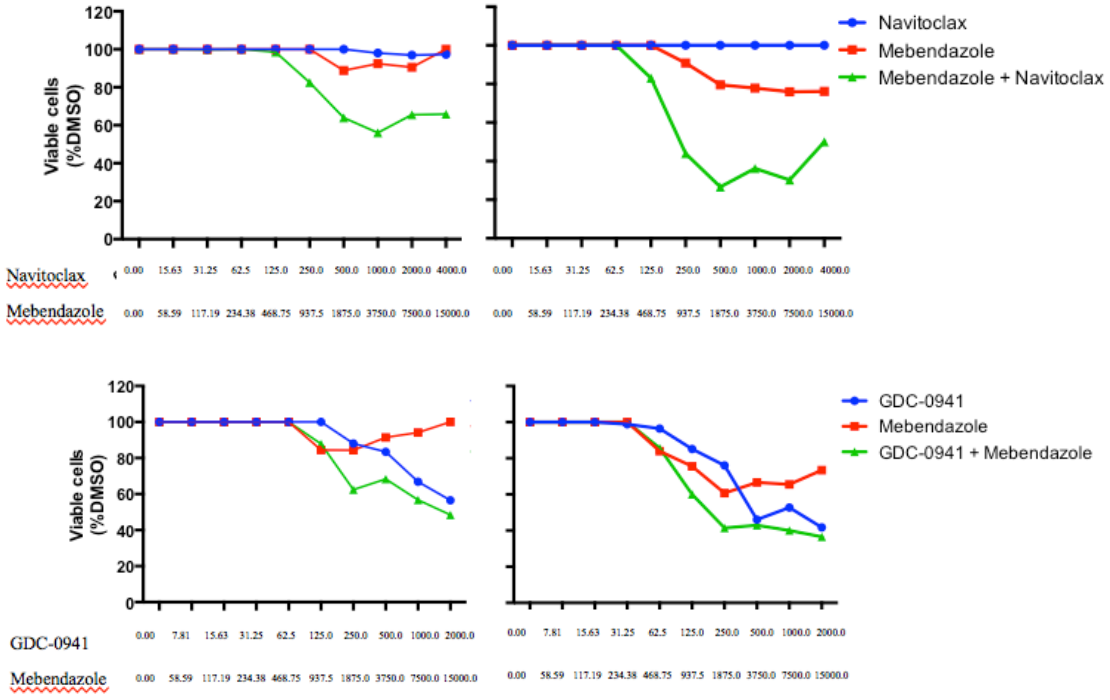

JHH-136 JHH-520

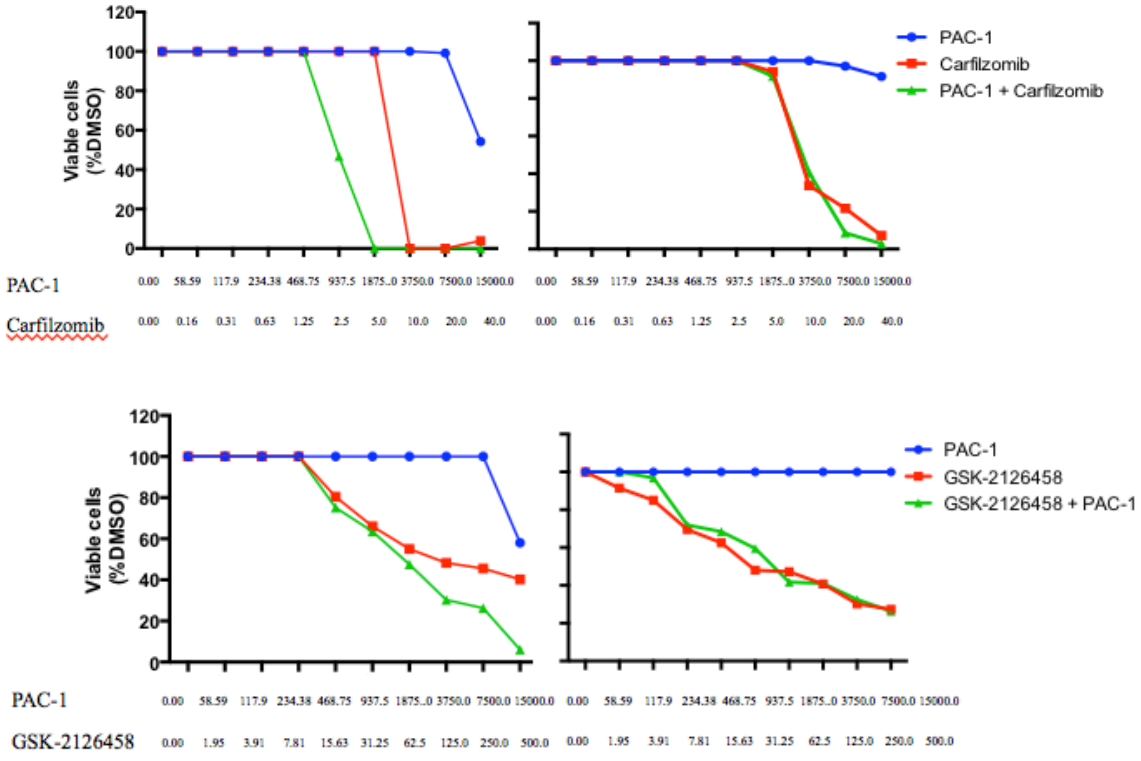

GDC-0941 paired with CNF-2024, PD0325901 or Marizomib extend survival *in vivo*

We wanted to determine whether the *in vitro* data could be replicated *in vivo*. The JHH-520 cell line was an excellent candidate for *in vivo* experimentation. This cell line was used in the 10x10 matrix experiments and has a MST of 82 days when implanted intracranially in nude mice. The xenograft tumors produced by JHH-520 are very invasive with areas of necrosis and mitotic figures. Next, we selected three drug combinations for testing *in vivo*.

Overall, GSK-2126458 was the only compound that could be combined synergistically with multiple drugs in either cell line therefore we chose to have a PIK3 inhibitor present in all combinations tested. GDC-0941 is a PIK3 inhibitor that was used in the drug combination matrix screen. Structurally, GDC-0941 and GSK-2126458 are dissimilar however they have a common target of the p110 subunit of PIK3. The largest difference between the two drugs is that GDC-0941 has some inhibition of mTOR but GSK-2126458 is a more potent mTOR inhibitor. GDC-0941 does penetrate the BBB, however the upper limit of how much drug gets into the brain is unknown (Salphati et al.). GDC-0941 was chosen to substitute for GSK-2126458.

Trametinib was a drug that was successful in combination with GDC-0941, however Trametinib has minimal BBB penetration (Gilmartin et al.). PD0325901 is a MEK inhibitor that is able to penetrate the BBB and has already been tested as a single agent in an intracranial GBM model (See et al.). CNF-2024 is an Hsp90 inhibitor with the ability to penetrate the BBB (confidential source) so this drug was selected for use in animal studies. Marizomib had evidence of brain penetration when given by intravenous

administration so this drug was consistent from the matrix screen to the in vivo testing (Williamson et al.),

The three combinations chosen were GDC-0941 paired with CNF-2024, PD0325901 or Marizomib. One control group was used for all three experiments. The GDC-0941 plus CNF-2024 treated group had a MST of 85 days compared to the untreated control group MST of 69 days (Figure 16). The MST of GDC-0941 plus Trametinib is 99.5 days, which is a significant improvement over the control group (Figure 16). The MST of GDC-0941 plus Marizomib is 104 days. Although the p value for this group was not significant, this was due to a single early mouse death. Additionally, this group had 2 of 5 animals live until termination of the experiment at 130 days with no outward signs of tumor. This data is excellent evidence that PIK3 inhibitors can be combined with a variety of drugs in vivo to extend survival.

Figure 16 (below). Drug combinations *in vivo* with GDC-0941 extend survival in JHH-520 model

Kaplan Meier curves for the JHH-520 model treated with control (vehicle) or GDC-0941 in combination with CNF-2024, PD325901 or Marizomib.

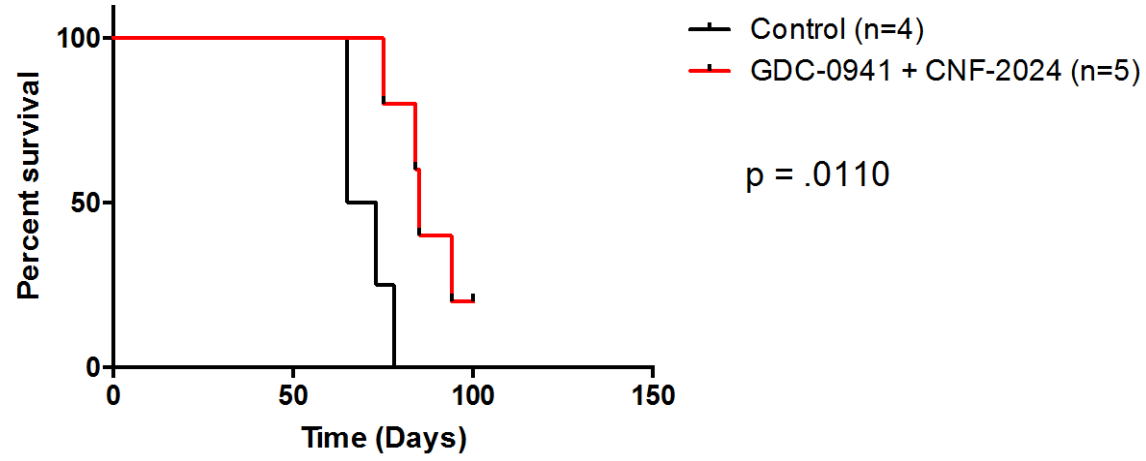
Control (n=4)
GDC-0941 + CNF-2024 (n=5)
p = .0110
Percent survival
100
50
0
0
50
100
150
Time (Days)

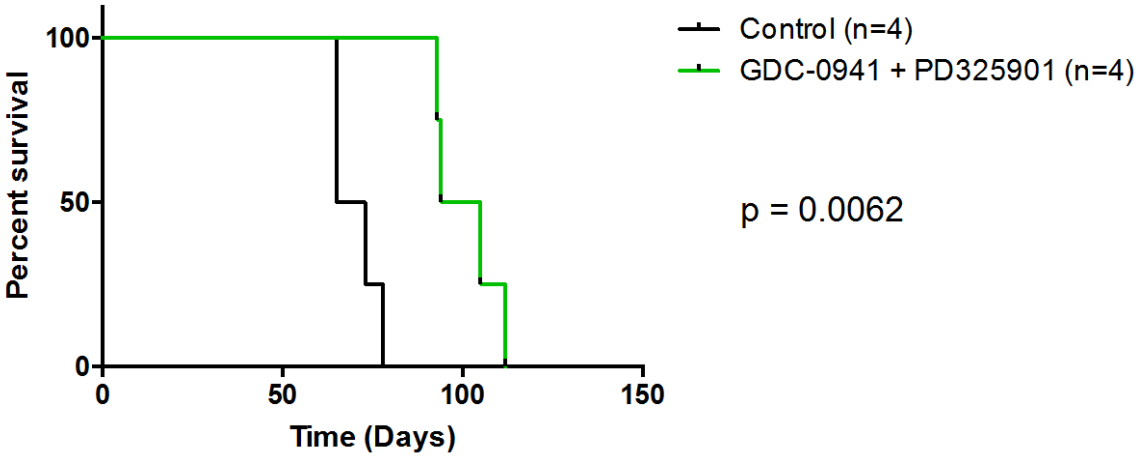
Control (n=4)
GDC-0941 + PD325901 (n=4)
p = 0.0062
Percent survival
100
50
0
0
50
100
150
Time (Days)

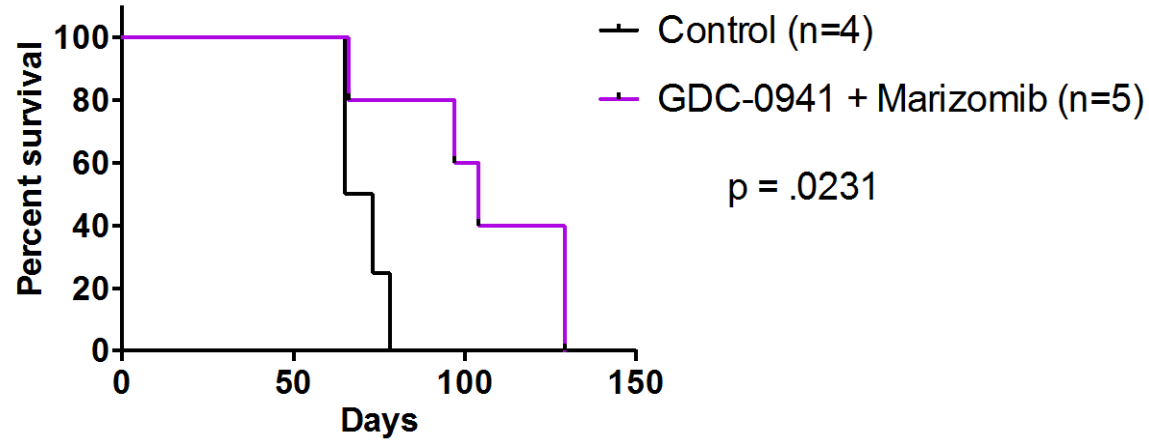
Control (n=4)
GDC-0941 + Marizomib (n=5)
p = .0231
Percent survival
100
80
60
40
20
0
0
50
100
150
Days

4 Discussion

Summary of Results

The purpose of this study was to develop a genomically characterized GBM oncosphere panel for *in vitro* and *in vivo* drug screening and development. We developed nine GBM oncosphere cell lines from patient derived tumors then determined the full genomic profile of each cell line. The genomic profile will be important to better interpret future research performed with these cell lines.

Next, we subjected two of these cell lines to a quantitative high throughput drug screen using a drug library composed of drugs proven to be effective in a variety of cancers. This study also provides additional evidence that oncospheres are amenable to a high throughput format, in addition to previous studies (Hothi et al.). We validated the hits in a non-high throughput format in additional oncosphere cell lines and found that

drug response differed depending on the cell line, perhaps due to the different driver mutation profiles. This data supports previous observations that cell line characteristics alter drug efficacy and underscore that genomic data should be used to inform future drug studies and clinical trials.

In vivo testing of CNF-2024 and Bardoxolone methyl failed to extend survival in the Br23C model. This data is evidence that single agent efficacy *in vitro* is difficult to replicate *in vivo* due to issues of toxicity, therapeutic window and brain penetration of the drug. Finally, we completed further drug combination screening using a novel qHTS matrix format. We found that PI3K inhibitors were synergistic with a variety of compounds in both cell lines tested. We selected compounds for animal testing by researching the ability of the compound to penetrate the BBB. Animal studies revealed that GDC-0941 in combination with three different drugs was able to extend survival in the JHH-520 model. This data is shows that careful consideration must be taken to assess the PK/PD properties of drugs prior to therapeutic testing. Overall, this project shows that our oncosphere cell lines are suitable for use *in vitro* and *in vivo* for therapeutic testing.

Each Oncosphere Cell Line is a Unique, Independent GBM Model

Genetic alterations common in primary GBM tissue has been widely studied and genes that likely drive GBM formation and growth have been determined (Parsons et al.; McLendon et al.). We found that our GBM oncosphere cell lines have alterations in GBM driver genes at similar frequencies to studies using primary tissue. The most common alterations we found were loss of *CDKN2A* and *PTEN,* the latter resulting in uncontrolled cell growth and overactive signaling through the PI3K/AKT pathway. Only two of our

cell lines contained *EGFR* amplification, which is a lower frequency than reported in primary tumor samples, suggesting a selection bias. It has been well documented that *EGFR* amplification and alterations are difficult to maintain in cell culture (Chen et al.). Many of our cell lines contained *NF1* alterations which causes overactive signaling through the Ras/MAPK pathway. This could be due to selective pressure for maintaining mutations that are advantageous for growth in culture. When protein expression was verified by western blot, we found a few inconsistencies to the sequencing data. These could be explained by epigenetic silencing mechanisms, mutations not considered in regulatory regions or other unforeseen mutational affects resulting in a loss of protein expression.

Previous studies show that GBM oncospheres grown in serum free conditions better maintain the parent tumor genomic mutation profile, than adherent cell lines grown with serum. Additionally, our GBM oncosphere cell lines can form intracranial tumors, which contain features of human GBM such as invasive growth and areas of necrosis. The use of U87MG, U251 and other adherent GBM cell lines lack the ability to form tumors *in vivo* that resemble human GBM which makes them a poor model for pre-clinical studies used to inform clinical trials. We hope that through widespread use of our GBM oncosphere panel, there can be pre-clinical studies done to inform successful clinical trials to improve treatment options for GBM patients.

Drug Efficacy can be dictated by the Characteristics of the Model Tested

Our qHTS study revealed a number of different drug classes that were effective at stopping GBM cell growth. We utilized two oncosphere cell lines with two different mutation profiles and found that EGFR inhibitors, NF-κB inhibitors, apoptosis activators

and epigenetic modulators were effective in both cell lines tested. When examining hits that were effective in JHH-136, a PTEN null and *NF1* wild type cell line, EGFR inhibitors were the only dominant drug class. For JHU-1016B, a PTEN mutant and NF1 null cell line, dominating drug classes were VEGFR, mTOR, PI3K inhibitors and Cdk/Chk inhibitors. This difference in the type and amount of effective inhibitors was unexpected. This study shows that genomic alterations in GBM driver genes can greatly affect drug efficacy.

The drug combination studies revealed similar results as the single agent studies. Most drugs selected for use in the combination matrix screen were effective in both JHH-136 and JHU-1016B, however when drug combinations were tested in JHH-520, there were differences in synergy. We believe this is due to the differences in the genomic mutation profile of JHH-136 and JHH-520. The drug combinations involving GSK-2126458, a PIK3 inhibitor, were the only combinations that showed maximal inhibition through synergy rather than extreme efficacy of a single agent within the combination. Other drug combinations involving highly efficacious single agents had maximal inhibition but synergy was minimal. This result was unexpected. This distinction is critical for future studies with drug combinations in humans.

The animal studies using single agents were unsuccessful. The common result is further evidence that *in vitro* efficacy does not always translate to *in vivo* efficacy. There are a number of reasons why *in vivo* efficacy is difficult to predict. This could be due to the differences in the models used for screening compared to *in vivo* testing. Also, our use of intracranial GBM models adds an additional hurdle of the drugs ability to cross the

BBB. CNF-2024 has published data showing that it is able to cross the BBB while Bardoxolone methyl has no findings published in this area.

Another interesting finding from the drug combination studies was which types of drugs could be paired together to produce maximal inhibition. GDC-0941 has been shown to cross the BBB (Salphati et al.) and has been tested in other cancers (Sos et al.; Hoeflich et al.) (Munugalavadla et al.), including glioma (Raynaud et al.). This compound is currently in multiple clinical trials for solid tumors. CNF-2024 or BIIB021 is a novel Hsp90 inhibitor with some ability to cross the BBB and recently completed Phase I clinical trials (Saif et al.). PD325901 has been tested as a single agent in an intracranial GBM model and showed a survival benefit (See et al.). Marizomib is a compound produced by a marine bacteria, *Salinispora tropica*, and is currently in Phase I/II clinical trials. Marizomib's ability to cross the BBB is somewhat controversial (Williamson et al.; Singh et al.). The significant survival benefit seen in all three of the combinations tested was surprising however, in hindsight our selection of compounds with evidence of crossing the BBB must have played a major role. Additionally, we used the same model *in vitro* and *in vivo,* which could also explain the success of all three combinations. Further experiments must be done to determine if the survival extension is due to drug synergy or single agent efficacy.

Future Directions

A large number of pre-clinical studies can be generated from this work. Various EGFR inhibitors have been tested in clinical trials as single agents and in combination with other drugs however, they have yet to show improvement of GBM patient survival. NF-κB inhibitors and apoptotic activators have not been widely tested on GBM. Further

studies should be done to test these classes of drug in GBM models *in vivo.* This data can also be used to inform studies regarding drug combinations that will be successful in the clinic.

The successful drug combinations we tested must be further explored to determine if the survival benefit is due to single agent efficacy or drug combination synergy. Once this has been determined we will attempt to move forward with clinical trials for GBM patients using the successful drug or drug combinations.

Summary

Our study is evidence that our glioma oncosphere cell line panel is a suitable model for *in vitro* and *in vivo* testing of GBM therapeutics. Our study also highlights the importance of the mutation profile of each individual patient tumor and how this can predict drug efficacy. We hope that this study will lead to improved drug combinations that will significantly increase the survival times for GBM patients.

REFERENCES

Actor, Bertrand et al. "Comprehensive Analysis of Genomic Alterations in Gliosarcoma and Its Two Tissue Components.." *Genes, chromosomes & cancer* 34.4 (2002): 416–427. Web.

Andjelkovic, M. et al. "Role of Translocation in the Activation and Function of Protein Kinase B." *J Biol Chem* 272.50 (1997): 31515–31524. Print.

Bai, Ren-Yuan et al. "Antiparasitic Mebendazole Shows Survival Benefit in 2 Preclinical Models of Glioblastoma Multiforme.." *Neuro Oncol* 13.9 (2011): 974–982. Web.

Bakir, A et al. "Establishment and Characterization of a Human Glioblastoma Multiforme Cell Line.." *Cancer genetics and cytogenetics* 103.1 (1998): 46–51. Print.

Biggs, W. H. 3rd, W. K. Cavenee, and K. C. Arden. "Identification and Characterization of Members of the FKHR (FOX O) Subclass of Winged-Helix Transcription Factors in the Mouse." *Mamm Genome* 12.6 (2001): 416–425. Web.

Bos, Johannes L. "The Ras Gene Family and Human Carcinogenesis." *Mutation Research/Reviews in Genetic Toxicology* 195.3 (1988): 255–271. Web.

Broderick, D. K. et al. "Mutations of PIK3CA in Anaplastic Oligodendrogliomas, High-Grade Astrocytomas, and Medulloblastomas." *Cancer Research* 64.15 (2004): 5048–5050. Web.

Brownawell, A. M. et al. "Inhibition of Nuclear Import by Protein Kinase B (Akt) Regulates the Subcellular Distribution and Activity of the Forkhead Transcription Factor AFX." *Mol Cell Biol* 21.10 (2001): 3534–3546. Web.

Cai, S. L. et al. "Activity of TSC2 Is Inhibited by AKT-Mediated Phosphorylation and Membrane Partitioning." *J Cell Biol* 173.2 (2006): 279–289. Web.

Chen, Ruihuan et al. "A Hierarchy of Self-Renewing Tumor-Initiating Cell Types in Glioblastoma.." *Cancer Cell* 17.4 (2010): 362–375. Web.

Cheney, I. W. et al. "Suppression of Tumorigenicity of Glioblastoma Cells by Adenovirus-Mediated MMAC1/PTEN Gene Transfer." *Cancer Research* 58.11 (1998): 2331–2334. Print.

Chi, Shunji, and Chifumi Kiatanka. "Oncogenic Ras Triggers Cell Suicide Through the Activation of a Caspase-Independent Cell Death Program in Human Cancer Cells." *Oncogene* 18.13 (1999): –. Web.

Cruickshanks, Nichola et al. "Lapatinib and Obatoclax Kill Tumor Cells Through Blockade of ERBB1/3/4 and Through Inhibition of BCL-XL and MCL-1.." *Molecular pharmacology* 81.5 (2012): 748–758. Web.

Datta, S. R. et al. "Akt Phosphorylation of BAD Couples Survival Signals to the Cell-Intrinsic Death Machinery." *Cell* 91.2 (1997): 231–241. Print.

Davies, Helen et al. "Mutations of the BRAF Gene in Human Cancer." *Nature* 417.6892 (2002): 949–954. Web.

Davies, M. A. et al. "Adenoviral Transgene Expression of MMAC/PTEN in Human Glioma Cells Inhibits Akt Activation and Induces Anoikis." *Cancer Res* 58.23 (1998): 5285–5290. Print.

DeAngelis, L. M. "Brain Tumors." *N Engl J Med* 344.2 (2001): 114–123. Web.

Denny, B J et al. "NMR and Molecular Modeling Investigation of the Mechanism of Activation of the Antitumor Drug Temozolomide and Its Interaction with DNA.."

Biochemistry 33.31 (1994): 9045–9051. Print.
Di Tomaso, E et al. "Establishment and Characterization of a Human Cell Line From Paediatric Cerebellar Glioblastoma Multiforme.." *Neuropathol Appl Neurobiol* 26.1 (2000): 22–30. Print.
Diehl, J. A. et al. "Glycogen Synthase Kinase-3beta Regulates Cyclin D1 Proteolysis and Subcellular Localization." *Genes Dev* 12.22 (1998): 3499–3511. Print.
Dudek, H. et al. "Regulation of Neuronal Survival by the Serine-Threonine Protein Kinase Akt." *Science* 275.5300 (1997): 661–665. Print.
el-Azouzi, M et al. "Loss of Distinct Regions on the Short Arm of Chromosome 17 Associated with Tumorigenesis of Human Astrocytomas." *Proc Natl Acad Sci U S A* (1989): n. pag. Print.
Evanthia Galanis et al. "Clinical Outcome of Gliosarcoma Compared with Glioblastoma Multiforme: North Central Cancer Treatment Group Results." *dx.doi.org* n. pag. Print.
Galli, Rossella et al. "Isolation and Characterization of Tumorigenic, Stem-Like Neural Precursors From Human Glioblastoma.." *Cancer Res* 64.19 (2004): 7011–7021. Web.
Gallia, G. L., S. Brem, and H. Brem. "Local Treatment of Malignant Brain Tumors Using Implantable Chemotherapeutic Polymers." *J Natl Compr Canc Netw* 3.5 (2005): 721–728. Print.
Gallia, Gary L et al. "Inhibition of Akt Inhibits Growth of Glioblastoma and Glioblastoma Stem-Like Cells.." *Molecular cancer therapeutics* 8.2 (2009): 386–393. Web.
Gilmartin, Aidan G et al. "GSK1120212 (JTP-74057) Is an Inhibitor of MEK Activity and Activation with Favorable Pharmacokinetic Properties for Sustained in Vivo Pathway Inhibition.." *Clinical cancer research : an official journal of the American Association for Cancer Research* 17.5 (2011): 989–1000. Web.
Griner, Lesley A Mathews et al. "High-Throughput Combinatorial Screening Identifies Drugs That Cooperate with Ibrutinib to Kill Activated B-Cell–Like Diffuse Large B-Cell Lymphoma Cells." *Proc Natl Acad Sci U S A* n. pag. Print.
Guha, A et al. "Proliferation of Human Malignant Astrocytomas Is Dependent on Ras Activation.." *Oncogene* 15.23 (1997): 2755–2765. Print.
Hartmann, C. et al. "PIK3CA Mutations in Glioblastoma Multiforme." *Acta Neuropathol* 109.6 (2005): 639–642. Web.
Hoeflich, K. P. et al. "Intermittent Administration of MEK Inhibitor GDC-0973 Plus PI3K Inhibitor GDC-0941 Triggers Robust Apoptosis and Tumor Growth Inhibition." *Cancer Research* 72.1 (2012): 210–219. Web.
Holland, E. C. et al. "Combined Activation of Ras and Akt in Neural Progenitors Induces Glioblastoma Formation in Mice." *Nat Genet* 25.1 (2000): 55–57. Web.
Hothi, Parvinder et al. "High-Throughput Chemical Screens Identify Disulfiram as an Inhibitor of Human Glioblastoma Stem Cells." *Oncotarget* 3.10 (2012): 1124–1136. Print.
Ignatova, Tatyana N et al. "Human Cortical Glial Tumors Contain Neural Stem-Like Cells Expressing Astroglial and Neuronal Markers in Vitro." *Glia* 39.3 (2002): 193–206. Web.
Inglese, James et al. "Quantitative High-Throughput Screening: a Titration-Based

Approach That Efficiently Identifies Biological Activities in Large Chemical Libraries..” *Proc Natl Acad Sci U S A* 103.31 (2006): 11473–11478. Web.
Jeuken, Judith et al. “RAS/RAF Pathway Activation in Gliomas: the Result of Copy Number Gains Rather Than Activating Mutations..” *Acta Neuropathol* 114.2 (2007): 121–133. Web.
Joensuu, H. et al. “Amplification of Genes Encoding KIT, PDGFRalpha and VEGFR2 Receptor Tyrosine Kinases Is Frequent in Glioblastoma Multiforme.” *J Pathol* 207.2 (2005): 224–231. Web.
Joshi, Avadhut D et al. “Evaluation of Tyrosine Kinase Inhibitor Combinations for Glioblastoma Therapy..” *PLoS One* 7.10 (2012): e44372. Web.
Knight, Steven D et al. “Discovery of GSK2126458, a Highly Potent Inhibitor of PI3K and the Mammalian Target of Rapamycin.” *ACS Medicinal Chemistry Letters* 1.1 (2010): 39–43. Web.
Knobbe, C. B., A. Trampe-Kieslich, and G. Reifenberger. “Genetic Alteration and Expression of the Phosphoinositol-3-Kinase/Akt Pathway Genes PIK3CA and PIKE in Human Glioblastomas.” *Neuropathol Appl Neurobiol* 31.5 (2005): 486–490. Web.
Knobbe, Christiane B, Julia Reifenberger, and Guido Reifenberger. “Mutation Analysis of the Ras Pathway Genes NRAS, HRAS, KRAS and BRAF in Glioblastomas..” *Acta Neuropathol* 108.6 (2004): 467–470. Web.
Lai, A. et al. “Phase II Study of Bevacizumab Plus Temozolomide During and After Radiation Therapy for Patients with Newly Diagnosed Glioblastoma Multiforme.” *J Clin Oncol* 29.2 (2010): 142–148. Web.
Lee, Jeongwu et al. “Tumor Stem Cells Derived From Glioblastomas Cultured in bFGF and EGF More Closely Mirror the Phenotype and Genotype of Primary Tumors Than Do Serum-Cultured Cell Lines.” *Cancer Cell* 9.5 (2006): 391–403. Web.
Lee, Seung-Rock et al. “Reversible Inactivation of the Tumor Suppressor PTEN by H2O2..” *J Biol Chem* 277.23 (2002): 20336–20342. Web.
Lefrou, Laurent et al. “[Germline Tp53 Neomutation in a Patient with Li-Fraumeni Syndrome and Pancreatic Adenocarcinoma]..” *Gastroentérologie clinique et biologique* 30.3 (2006): 484–486. Print.
Li, J., C. Yen, et al. “PTEN, a Putative Protein Tyrosine Phosphatase Gene Mutated in Human Brain, Breast, and Prostate Cancer.” *Science* 275.5308 (1997): 1943–1947. Print.
Li, J., L. Simpson, et al. “The PTEN/MMAC1 Tumor Suppressor Induces Cell Death That Is Rescued by the AKT/Protein Kinase B Oncogene.” *Cancer Res* 58.24 (1998): 5667–5672. Print.
Loilome, Watcharin et al. “Glioblastoma Cell Growth Is Suppressed by Disruption of Fibroblast Growth Factor Pathway Signaling..” *Journal of neuro-oncology* 94.3 (2009): 359–366. Web.
Louis, David N et al. “The 2007 WHO Classification of Tumours of the Central Nervous System..” *Acta Neuropathol* 114.2 (2007): 97–109. Web.
Lyustikman, Yelena et al. “Constitutive Activation of Raf-1 Induces Glioma Formation in Mice..” *Neoplasia (New York, N.Y.)* 10.5 (2008): 501–510. Print.
Maehama, T., and J. E. Dixon. “The Tumor Suppressor, PTEN/MMAC1, Dephosphorylates the Lipid Second Messenger, Phosphatidylinositol 3,4,5-Trisphosphate.” *J Biol Chem* 273.22 (1998): 13375–13378. Print.

Mathews, Lesley A et al. “A 1536-Well Quantitative High-Throughput Screen to Identify Compounds Targeting Cancer Stem Cells..” *Journal of biomolecular screening* 17.9 (2012): 1231–1242. Web.

Mayo, L. D., and D. B. Donner. “A Phosphatidylinositol 3-Kinase/Akt Pathway Promotes Translocation of Mdm2 From the Cytoplasm to the Nucleus.” *Proc Natl Acad Sci U S A* 98.20 (2001): 11598–11603. Web.

McLendon, Roger et al. “Comprehensive Genomic Characterization Defines Human Glioblastoma Genes and Core Pathways.” *Nature* 455.7216 (2008): 1061–1068. Web.

Morrison, R. S., F. Yamaguchi, et al. “Fibroblast Growth Factor Receptor Gene Expression and Immunoreactivity Are Elevated in Human Glioblastoma Multiforme.” *Cancer Res* 54.10 (1994): 2794–2799. Print.

Morrison, R. S., S. Giordano, et al. “Basic Fibroblast Growth Factor Expression Is Required for Clonogenic Growth of Human Glioma Cells.” *J Neurosci Res* 34.5 (1993): 502–509. Web.

Mueller, W. et al. “Mutations of the PIK3CA Gene Are Rare in Human Glioblastoma.” *Acta Neuropathol* 109.6 (2005): 654–655. Web.

Munugalavadla, V et al. “The PI3K Inhibitor GDC-0941 Combines with Existing Clinical Regimens for Superior Activity in Multiple Myeloma.” *Oncogene* (2013): –. Web.

Parsons, D Williams et al. “An Integrated Genomic Analysis of Human Glioblastoma Multiforme..” *Science* 321.5897 (2008): 1807–1812. Web.

Perry, Arie et al. “Malignant Gliomas with Primitive Neuroectodermal Tumor-Like Components: a Clinicopathologic and Genetic Study of 53 Cases.” *Brain Pathology* 19.1 (2009): 81–90. Web.

Peterson, Quinn P et al. “Procaspase-3 Activation as an Anti-Cancer Strategy: Structure-Activity Relationship of Procaspase-Activating Compound 1 (PAC-1) and Its Cellular Co-Localization with Caspase-3..” *J Med Chem* 52.18 (2009): 5721–5731. Web.

Rand, V. et al. “Sequence Survey of Receptor Tyrosine Kinases Reveals Mutations in Glioblastomas.” *Proc Natl Acad Sci U S A* 102.40 (2005): 14344–14349. Web.

Rao, S. K. et al. “A Survey of Glioblastoma Genomic Amplifications and Deletions.” *Journal of neuro-oncology* 96.2 (2009): 169–179. Web.

Raynaud, Florence I et al. “Biological Properties of Potent Inhibitors of Class I Phosphatidylinositide 3-Kinases: From PI-103 Through PI-540, PI-620 to the Oral Agent GDC-0941.” *Molecular cancer therapeutics* (2009): n. pag. Print.

Reilly, Karlyne M et al. “Nf1;Trp53 Mutant Mice Develop Glioblastoma with Evidence of Strain-Specific Effects.” *Nat Genet* 26.1 (2000): 109–113. Web.

Robinson, J P et al. “Activated BRAF Induces Gliomas in Mice When Combined with Ink4a/Arf Loss or Akt Activation.” *Oncogene* 29.3 (2009): 335–344. Web.

Saif, Muhammad Wasif et al. “Stressing the Development of Small Molecules Targeting HSP90.” *Clinical Cancer Research* 20.2 (2014): 275–277. Web.

Salphati, L et al. “Role of P-Glycoprotein and Breast Cancer Resistance Protein-1 in the Brain Penetration and Brain Pharmacodynamic Activity of the Novel Phosphatidylinositol 3-Kinase Inhibitor GDC-0941.” *Drug Metabolism and Disposition* 38.9 (2010): 1422–1426. Web.

Samuels, Y. et al. “High Frequency of Mutations of the PIK3CA Gene in Human Cancers.” *Science* 304.5670 (2004): 554. Web.
Santini, Maria Teresa, and Gabriella Rainaldi. “Three-Dimensional Spheroid Model in Tumor Biology.” *Pathobiology* 67.3 (1999): 148–157. Web.
Schwarz, Jana Marie et al. “MutationTaster Evaluates Disease-Causing Potential of Sequence Alterations..” *Nature methods* 7.8 (2010): 575–576. Web.
See, W L et al. “Sensitivity of Glioblastomas to Clinically Available MEK Inhibitors Is Defined by Neurofibromin 1 Deficiency.” *Cancer Research* 72.13 (2012): 3350–3359. Web.
Singh, Ajita V et al. “Pharmacodynamic and Efficacy Studies of the Novel Proteasome Inhibitor NPI-0052 (Marizomib) in a Human Plasmacytoma Xenograft Murine Model.” *British Journal of Haematology* 149.4 (2010): 550–559. Web.
Siu, I-Mei et al. “Establishment of a Human Glioblastoma Stemlike Brainstem Rodent Tumor Model..” *Journal of neurosurgery. Pediatrics* 6.1 (2010): 92–97. Web.
Sos, M L et al. “Identifying Genotype-Dependent Efficacy of Single and Combined PI3K- and MAPK-Pathway Inhibition in Cancer.” *Proceedings of the National Academy of Sciences* 106.43 (2009): 18351–18356. Web.
Stiles, B. et al. “Essential Role of AKT-1/Protein Kinase B Alpha in PTEN-Controlled Tumorigenesis.” *Mol Cell Biol* 22.11 (2002): 3842–3851. Print.
Stupp, R. et al. “Radiotherapy Plus Concomitant and Adjuvant Temozolomide for Glioblastoma.” *N Engl J Med* 352.10 (2005): 987–996. Web.
Sun, M. et al. “AKT1/PKBalpha Kinase Is Frequently Elevated in Human Cancers and Its Constitutive Activation Is Required for Oncogenic Transformation in NIH3T3 Cells.” *Am J Pathol* 159.2 (2001): 431–437. Print.
Tamura, M. “Inhibition of Cell Migration, Spreading, and Focal Adhesions by Tumor Suppressor PTEN.” *Science* 280.5369 (1998): 1614–1617. Web.
Thiel, G et al. “Somatic Mutations in the Neurofibromatosis 1 Gene in Gliomas and Primitive Neuroectodermal Tumours..” *Anticancer research* 15.6B (1995): 2495–2499. Print.
Wakimoto, Hiroaki et al. “Maintenance of Primary Tumor Phenotype and Genotype in Glioblastoma Stem Cells..” *Neuro Oncol* 14.2 (2012): 132–144. Web.
Walker, M. D. et al. “Randomized Comparisons of Radiotherapy and Nitrosoureas for the Treatment of Malignant Glioma After Surgery.” *N Engl J Med* 303.23 (1980): 1323–1329. Web.
Williamson, Mark et al. “Comparison of Biochemical and Biological Effects of ML858 (Salinosporamide a) and Bortezomib.” *Molecular cancer therapeutics* 5.12 (2006): 3052–3061. Web.
Wong, A. J. et al. “Structural Alterations of the Epidermal Growth Factor Receptor Gene in Human Gliomas.” *Proc Natl Acad Sci U S A* 89.7 (1992): 2965–2969. Print.
Yasgar et al. “Compound Management for Quantitative High-Throughput Screening..” *Journal of the Association for Laboratory Automation* 13.2 (2008): 79–89. Web.
Zhu, Yuan et al. “Early Inactivation of P53 Tumor Suppressor Gene Cooperating with NF1 Loss Induces Malignant Astrocytoma.” *Cancer Cell* 8.2 (2005): 119–130. Web.

CURRICULUM VITAE

Kelli M. Wilson

March, 2014

DEMOGRAPHIC INFORMATION

Current Position: Doctoral Candidate, Cellular and Molecular Medicine Graduate Program, Department of Pathology, Johns Hopkins University School of Medicine.

Business address:

Cancer Research Building II

1550 Orleans Street, Room 276

Baltimore, MD 21287

Tele: 410-502-9608

Fax: 410-502-5559

E-mail: kmcdowe5@jhmi.edu

Date of birth: March 17, 1984

EDUCATION

August 2002 – May 2006: BS in Biological Sciences at North Carolina State University, Raleigh NC

August 2008 – present: Graduate Student in Cellular and Molecular Medicine Graduate Program, Department of Neurosurgery, Johns Hopkins School of Medicine, Baltimore, MD (Advisor: Dr. Gregory Riggins, Program Director: Dr. Rajini Rao).

PUBLICATIONS IN PEER REVIEWED JOURNALS

1. ***McDowell, K. A**., Riggins, G. J., & Gallia, G. L. (2011). Targeting the AKT Pathway in Glioblastoma. *Current pharmaceutical design***.** 17(23): 2411-20.
2. ***McDowell, K. A**., Hutchinson, A. N., Wong-Goodrich, S. J. E., Presby, M. M., Su, D., Rodriguez, R. M., Law, K. C., et al. (2010). Reduced Cortical BDNF Expression and Aberrant Memory in Carf Knock-Out Mice. *The Journal of neuroscience. 30*(22), 7453–7465.

ABSTRACTS

1. **Wilson, K. M.**, Mathews L.A., Thomas C.J., Keller J.M., Shinn P., McKnight C., et al. (2013). A Quantitative High Throughput Drug Screen Based on a Glioma Oncosphere Panel. National Graduate Student Research Conference, Bethesda, MD.

RELATED RESEARCH

Research in the Entomology laboratory of Dr. Fred Gould

North Carolina State University: October 2003 - June 2006

Honors Project Summary: Effects of Inbreeding on a Population of *Heliothis subflexa* Moths

Techniques: PCR, RFLP analysis, moth mating, moth dissection, moth colony maintenance

Research in the Neuroscience laboratory of Dr. Anne E. West

Duke University: October 2006 - June 2008

Project Summary: Characterization of Activity Dependent Transcription of BDNF in a Carf Knock out mouse

Techniques: molecular cloning, cell culture, cellular transfection, lentiviral production, siRNA, protein binding, RT-PCR, electrophoretic mobility shift assays, mouse dissection, mouse surgeries, mouse drug administration

TEACHING EXPERIENCE

Medical Student course (Teaching Assistant):

Johns Hopkins School of Medicine – Baltimore, MD

Course Discussion – October 2013

Cell Physiology

Undergraduate immunology course (Adjunct professor):

University of the District of Columbia – Washington, DC

Course Taught – Spring 2013

BIO346: Immunology Lecture

BIO344: Immunology Lab

INSTITUTIONAL ORGANIZATION ACTIVITIES

Johns Hopkins Biomedical Scholars Association –

2009-2010: Activities Coordinator

Johns Hopkins Student National Medical Association –

2009-2010: Community Service Coordinator

MEMBERSHIP IN PROFESSIONAL SOCIETIES

2010-present: Association for Women in Science (AWIS), Greater Baltimore Chapter

VOLUNTEER/ACTIVITIES

Incentive Mentoring Program, Division Leader - 2008-2013

Organization Background: 501(c)(3) organization which engages Baltimore City high school students who have a failing GPA during freshmen year and are facing significant challenges outside the classroom by providing each student with a team of committed volunteers for a period of eight years

Duties: Managed two teams of 5-10 volunteers who mentor high school and college students**,** Proposed creative solutions to reach short and long term goals for volunteers and students**,** managed crisis events in student's lives by connecting families with community resources**,** Responsible for managing tutoring sessions for 32 high school students, two days a week for 4 years**,** composed biannual reports on tutoring attendance with recommendations to volunteers to increase student attendance**,** Designed and implemented the IMP Wiki, an online collaborative resource for volunteers, which details procedures and information necessary to handle routine and unexpected crisis situations with students**,** Administrator for online summer school classes for 35 students, responsible for student registration, progress monitoring, volunteer training and grade validation**,** Responsible for increasing visibility of the organization to the public through social media, newsletter editing, photo collection and donor recognition

Outcomes: Three mentees are currently in college at Bowie State University and Community College of Baltimore College, one mentee has completed his BS in Criminal Justice at California University of Pennsylvania, one mentee is graduating from high school in 2014

Johns Hopkins University School of Medicine, Fun with Science Summer Camp
Counselor, Summer of 2012 and 2013

Duties: Coordinated daily learning and experimental activities for over 20 5th graders**,** Supervised student activities and experiments using microscopy, fluorescent bacteria, crystals, forensic science and chemistry**,** Assisted daily speakers with set up and monitoring student activities